Impact of disorder on the superconducting transition temperature near a Lifshitz transition

Thaís V. Trevisan,[1,2] Michael Schütt,[1] and Rafael M. Fernandes[1]
[1]*School of Physics and Astronomy, University of Minnesota, Minneapolis, Minnesota 55455, USA*
[2]*Instituto de Física Gleb Wataghin, Unicamp, Rua Sérgio Buarque de Holanda, 777, CEP 13083-859 Campinas, SP, Brazil*

(Received 5 April 2018; published 18 September 2018)

Multiband superconductivity is realized in a plethora of systems, from high-temperature superconductors to very diluted superconductors. While several properties of multiband superconductors can be understood as straightforward generalizations of their single-band counterparts, recent works have unveiled rather unusual behaviors unique to the former case. In this regard, a regime that has received significant attention is that near a Lifshitz transition, in which one of the bands crosses the Fermi level. In this paper, we investigate how impurity scattering τ^{-1} affects the superconducting transition temperature T_c across a Lifshitz transition, in the regime where intraband pairing is dominant and interband pairing is subleading. This is accomplished by deriving analytic asymptotic expressions for T_c and $\partial T_c/\partial\tau^{-1}$ in a two-dimensional two-band system. When the interband pairing interaction is repulsive, we find that, despite the incipient nature of the band crossing the Fermi level, interband impurity scattering is extremely effective in breaking Cooper pairs, making $\partial T_c/\partial\tau^{-1}$ quickly approach the limiting Abrikosov-Gor'kov value of the high-density regime. In contrast, when the interband pairing interaction is attractive, pair-breaking is much less efficient, affecting T_c only mildly at the vicinity of the Lifshitz transition. The consequence of this general result is that the behavior of T_c across a Lifshitz transition can be qualitatively changed in the presence of strong enough disorder: Instead of displaying a sharp increase across the Lifshitz transition, as in the clean case, T_c can actually display a maximum and be suppressed at the Lifshitz transition. These results shed light on the nontrivial role of impurity scattering in multiband superconductors.

DOI: 10.1103/PhysRevB.98.094514

I. INTRODUCTION

Just a few years after the development of the BCS theory of superconductivity, an extension of this model to multiband superconductors (SC) was proposed by Suhl *et al.* [1] and Moskalenko [2] to investigate the consequences of overlapping bands in the superconducting state of certain transition metals. Indeed, multiband superconductivity should be common among materials in which multiple electronic d orbitals are occupied, and whose crystal field splittings are not too large. Currently, there are many known multiband SC, ranging from conventional SC such as MgB_2 [3], $NbSn_3$ [4], and $NbSe_2$ [5], to unconventional SC such as $BaFe_2As_2$ [6], Sr_2RuO_4 [7], and $CeCoIn_5$ [8]. More recently, multiband superconductivity has been demonstrated in bulk $SrTiO_3$ [9,10] and in $LaAlO_3/SrTiO_3$ heterostructures [11], although the microscopic origin of superconductivity in these systems remains hotly debated [12–16]. Theoretically, several recent studies have unveiled unique properties of multiband SC that are not realized in their single-band counterparts [17–24].

An interesting regime in multiband SC is when one of the bands is incipient, i.e., its bottom (or top) is just below (or above) the Fermi level. The appearance or disappearance of a Fermi pocket from the Fermi surface is often called a Lifshitz transition (LT) [25]. Note that, in its original conception, a LT referred to a change in the topology of the Fermi surface from open to closed. However, given the widespread use of this term to also denote the situation of a band crossing the Fermi level, we will here use LT to refer to the latter case. Near a LT, the energy scale of the pairing interaction is larger than the Fermi energy of the incipient band, which may lead to interesting new behaviors [26–36].

Experimentally, tuning a multiband superconductor to a LT has been achieved by doping, gating, and even pressure. For instance, such a LT has been shown to take place in the phase diagrams of $Ba(Fe_{1-x}Co_x)_2As_2$ [37], pressurized KFe_2As_2 [38], $SrTiO_{3-\delta}$ [9], and gated $SrTiO_3/LaAlO_3$ [11]. Theoretically, the goal is to relate the thermodynamic properties of the SC across the LT transition with the microscopic properties of the gap function to shed light on the mechanisms involved in the pairing problem. Take, for instance, the case of $Ba(Fe_{1-x}Co_x)_2As_2$: The superconducting transition temperature T_c was found to vanish when the hole pockets sank below the Fermi level, indicating the dominance of interband pairing over intraband pairing [37]. The latter would be expected to dominate if the standard electron-phonon interaction was the pairing glue. The situation, however, is much less clear in $SrTiO_{3-\delta}$ and gated $LaAlO_3/SrTiO_3$ [9,11]: there, superconductivity is quite well established in the single-band regime, indicating dominant intraband pairing. However, T_c is actually suppressed across the LT, once the second band crosses the Fermi level. Such a behavior is at odds with general theoretical expectations that T_c should increase across a LT since the extra band provides more carriers to be part of the SC state [26,27,36].

In this paper, we investigate how disorder affects T_c and the gap functions across a two-band LT. We argue that the impact of disorder is fundamentally different depending on whether the interband pairing interaction is repulsive or attractive. In the former case, interband impurity scattering is strongly

 ©2018 American Physical Society

pair-breaking, implying that once the second band becomes part of the Fermi surface, pair-breaking effects become more substantial. Interestingly, crossing the LT leads to a change in the pairing symmetry from sign-changing gaps between the two bands to same-sign gaps [39]. These effects, in contrast, do not happen for an attractive interband interaction.

In our previous work [39], this problem was solved numerically in 3D and in 2D in the dirty limit, and applied to the particular cases of $SrTiO_{3-\delta}$ and gated $LaAlO_3/SrTiO_3$. Here, we instead focus on general analytical asymptotic results for small impurity scattering in 2D, which leads to important insights on the mechanisms involved. We obtain not only analytic expressions for T_c, but also for the rate of change of T_c with respect to interband impurity scattering τ_{inter}^{-1}, $\partial T_c/\partial \tau_{\text{inter}}^{-1}$. The latter is derived by using a technique based on Hellmann-Feynman theorem, following the seminal work of Ref. [40]. Starting in the high-density regime, where the system has long crossed the LT, we recover the well-known result for identical bands that $\partial T_c/\partial \tau_{\text{inter}}^{-1} = 0$ for attractive interband pairing (sign-preserving s^{++} superconducting state), and $\partial T_c/\partial \tau_{\text{inter}}^{-1} = -\pi/4$ (the universal Abrikosov-Gor'kov value) for repulsive interband scattering (sign-changing s^{+-} superconducting state). Deviations from this fine-tuned condition of identical bands with identical intraband pairing interactions leads to a reduction of the T_c suppression in the s^{+-} case, and an enhancement of the T_c suppression in the s^{++} case. When the system is well inside the single-band regime, i.e., well before crossing the LT, the suppression rate $\partial T_c/\partial \tau_{\text{inter}}^{-1}$ is very small regardless of the sign of the interband pairing. The interesting behavior takes place in the vicinity of the LT. For the s^{+-} state, we show that $\partial T_c/\partial \tau_{\text{inter}}^{-1}$ is strongly suppressed and quickly approaches the high-density value, even in the regime where the second band is only incipient. This contrasts to the behavior of the s^{++} state, in which $\partial T_c/\partial \tau_{\text{inter}}^{-1}$ has a small minimum at the LT before it increases towards the high-density value.

The paper is organized in the following way: to introduce the model, we start in Sec. II with a clean two-band superconductor, solving the pairing problem both numerically and analytically. In Sec. III, we generalize the model to include nonmagnetic random impurities. Section IV presents the analytic asymptotic solutions of the dirty superconductor across a LT both in the high-density regime and in the dilute regime. In Sec. V, we summarize our conclusions. Appendices A, B, and C provide more details about the analytic calculations performed in the main text.

II. CLEAN TWO-BAND SUPERCONDUCTOR

A. Gap equations

The two-band SC system that we study here is described by the Hamiltonian

$$H_0 = \sum_{\mathbf{k},i,\sigma} \xi_{i,\mathbf{k}}\, c^\dagger_{i,\mathbf{k}\sigma} c_{i,\mathbf{k}\sigma} + \sum_{\mathbf{k},\mathbf{k}',i,j} V_{ij} c^\dagger_{i,\mathbf{k}\uparrow} c^\dagger_{i,-\mathbf{k}\downarrow} c_{j,-\mathbf{k}'\downarrow} c_{j,\mathbf{k}'\uparrow}, \quad (1)$$

where $c^\dagger_{j,\mathbf{k}\sigma}$ and $c_{j,\mathbf{k}\sigma}$ are the operators that create and annihilate, respectively, an electron in band i ($i = 1,2$), with momentum $\mathbf{k}$ and spin σ. As in Refs. [27,39], we consider parabolic electronlike bands $\xi_{1,\mathbf{k}} = \frac{k^2}{2m_1} - \mu$ and $\xi_{2,\mathbf{k}} = \frac{k^2}{2m_2} - \mu + \varepsilon_0$, as illustrated in Fig. 1. The bottom of band 1, $W_1 = -\mu$, is split from the bottom of band 2, $W_2 = -\mu + \varepsilon_0$, by the energy scale $\varepsilon_0 > 0$. The chemical potential $\mu > 0$ is a control parameter in our model, which tunes the system through a LT at $\mu = \varepsilon_0$.

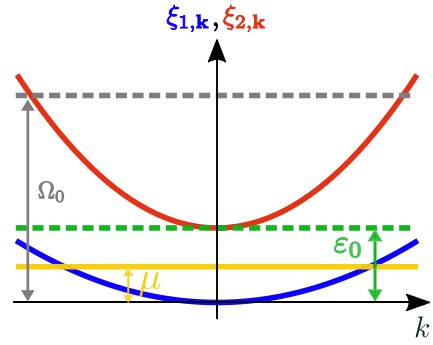

FIG. 1. Illustration of the two-band model used in this paper. Two electronlike parabolic and concentric bands are displaced by an energy $\varepsilon_0 > 0$. Their occupations are controlled by the chemical potential $\mu > 0$. When μ becomes larger than ε_0, the second band becomes populated, signaling a Lifshitz transition (LT).

The pairing interaction is described by the matrix V_{ij} and contains both (momentum-independent) intraband pairing, V_{11} and V_{22}, which do not need to be necessarily equal, and interband pairing, $V_{12} = V_{21}$. As a result, the isotropic SC gap Δ_i in band i is given by

$$\Delta_i = -\sum_{\mathbf{k},j} V_{ij} \langle c_{j,-\mathbf{k}\downarrow} c_{j,\mathbf{k}\uparrow} \rangle, \quad (2)$$

yielding the usual mean-field Hamiltonian:

$$H_0 = \sum_{\mathbf{k},i,\sigma} \xi_{i,\mathbf{k}}\, c^\dagger_{i,\mathbf{k}\sigma} c_{i,\mathbf{k}\sigma} - \sum_{\mathbf{k},i} (\Delta_i\, c^\dagger_{i,\mathbf{k}\uparrow} c^\dagger_{i,-\mathbf{k}\downarrow} + \text{H.c.}). \quad (3)$$

Before introducing disorder, we rederive the results for T_c of a clean two-band system across a LT (see also Ref. [27] and references therein). Introducing the Nambu spinor $\hat{\psi}^\dagger_{\mathbf{k}} = (c^\dagger_{1,\mathbf{k}\uparrow}\, c_{1,-\mathbf{k}\downarrow}\, c^\dagger_{2,\mathbf{k}\uparrow}\, c_{2,-\mathbf{k}\downarrow})$, we can readily obtain the normal and anomalous Green's functions of band i, $\mathcal{G}_i$ and $\mathcal{F}_i$, which appear in the Nambu's Green's function $\hat{\mathcal{G}}_0$ as

$$\hat{\mathcal{G}}_0(\mathbf{k},\omega_n) = \begin{pmatrix} \mathcal{G}_{1,0} & \mathcal{F}_{1,0} & 0 & 0 \\ \mathcal{F}_{1,0} & -\mathcal{G}^*_{1,0} & 0 & 0 \\ 0 & 0 & \mathcal{G}_{2,0} & \mathcal{F}_{2,0} \\ 0 & 0 & \mathcal{F}_{2,0} & -\mathcal{G}^*_{2,0} \end{pmatrix}. \quad (4)$$

We find

$$\mathcal{G}_{i,0}(\mathbf{k},\omega_n) = -\frac{i\omega_n + \xi_{i,\mathbf{k}}}{\omega_n^2 + \xi_{i,\mathbf{k}}^2 + \Delta_i^2}, \quad (5)$$

and

$$\mathcal{F}_{i,0}(\mathbf{k},\omega_n) = \frac{\Delta_i}{\omega_n^2 + \xi_{i,\mathbf{k}}^2 + \Delta_i^2}. \quad (6)$$

The latter is related to the pair expectation value, $\langle c_{i,-\mathbf{k}\downarrow} c_{i,\mathbf{k}\uparrow}\rangle = T\sum_n \mathcal{F}_{i,0}(\mathbf{k},\omega_n)$, from which we can derive the gap equation:

$$\Delta_i = \pi T \sum_{j,n} \lambda_{ij}\Delta_j \left\langle \frac{1}{\omega_n^2+\xi^2+\Delta_j^2}\right\rangle_j^{\Omega_0}. \tag{7}$$

Here, we introduced the dimensionless coupling constants $\lambda_{ij} = -\rho_{j,0}V_{ij}$, such that positive and negative λ_{ij} correspond to attraction and repulsion, respectively. We also defined the notation

$$\langle \mathcal{O}(\xi)\rangle_i^{\xi_c} \equiv \frac{1}{\pi\rho_{i,0}}\int_{W_i}^{\xi_c} d\xi \rho_i(\xi)\mathcal{O}(\xi), \tag{8}$$

where $\mathcal{O}(\xi)$ is an arbitrary function of energy, ξ_c denotes the upper cutoff of the integral, and W_i denotes the bottom of band i. In the gap equation, the upper limit of the integration corresponds to the energy cutoff of the pairing interaction, Ω_0, which plays a similar role as the Debye frequency in the standard BCS approach. Finally, $\rho_i(\xi)$ is the density of states per spin of band i, and $\rho_{i,0}\equiv\rho_i(W_i+\varepsilon_0)$. Since we have parabolic bands, $\rho_i(\xi) = \frac{m_i}{2\pi}$ for the 2D case and $\rho_i(\xi) = \frac{(2m_i)^{3/2}\sqrt{\varepsilon_0}}{4\pi^2}\sqrt{\frac{\xi-W_i}{\varepsilon_0}}$ for the 3D case, yielding $\rho_{i,0} = \frac{m_i}{2\pi}$ and $\rho_{i,0} = \frac{(2m_i)^{3/2}\sqrt{\varepsilon_0}}{4\pi^2}$, respectively. The linearized gap equation follows directly from Eq. (7):

$$\begin{pmatrix}\Delta_1\\ \Delta_2\end{pmatrix} = \begin{pmatrix}\lambda_{11} & \lambda_{12}\\ \lambda_{21} & \lambda_{22}\end{pmatrix}\hat{A}_{\text{clean}}(\mu,T_c)\begin{pmatrix}\Delta_1\\ \Delta_2\end{pmatrix}, \tag{9}$$

where $\hat{A}_{\text{clean}}$ has matrix elements:

$$\begin{aligned}(\hat{A}_{\text{clean}})_{ij} &= \delta_{ij}\pi T_c\sum_n \left\langle \frac{1}{\omega_n^2+\xi^2}\right\rangle_i^{\Omega_0}\\ &= \delta_{ij}\frac{\pi}{2}\left\langle \frac{1}{\xi}\tanh\left(\frac{\xi}{2T_c}\right)\right\rangle_i^{\Omega_0}.\end{aligned} \tag{10}$$

Equation (9) defines an eigenvalue problem. T_c, as a function of the chemical potential μ, is determined when the largest eigenvalue of $\hat{\lambda}\hat{A}_{\text{clean}}$ equals 1, where $(\hat{\lambda})_{ij} = \lambda_{ij}$. This is given by

$$\prod_{i=1,2}[(\hat{A}_{\text{clean}})_{ii}\det(\hat{\lambda}) - \lambda_{\bar{i}\bar{i}}] = \lambda_{12}\lambda_{21}, \tag{11}$$

as long as $\det(\hat{\lambda}) = \lambda_{11}\lambda_{22}-\lambda_{12}\lambda_{21}\neq 0$. Here, we introduced the notation $\bar{i} = 1(2)$ for $i = 2(1)$. It is clear that the equations depend only on the product $\lambda_{12}\lambda_{21}$, i.e., only on the square of the interband interaction V_{12}^2. As a result, $T_c(\mu)$ is independent of whether the interband pairing interaction is repulsive or attractive [27,36]. On the other hand, the sign of the off-diagonal term λ_{12} (which by definition is the same as the sign of λ_{21} and the opposite of V_{12}) determines the eigenvector corresponding to the largest eigenvalue of $\hat{\lambda}\hat{A}$. When $\lambda_{12}>0$, this eigenvector is such that Δ_1 and Δ_2 have the same sign, corresponding to a conventional s^{++} SC state. When $\lambda_{12}<0$, Δ_1 and Δ_2 acquire opposite signs, corresponding to an unconventional s^{+-} SC state

It is important to note that the chemical potential μ that appears in the gap equation is not the $T=0$ chemical potential, but actually $\mu(T_c)$. Close to the LT, because the Fermi energy is small, $\mu(T_c)$ can be different than $\mu(0)$ [29]. To avoid this issue, one can express the superconducting transition temperature as function of the total number of electrons in the system, N, which is given by

$$\begin{aligned}N &= 2\sum_{\mathbf{k}}\left[1 - T_c\sum_{j,n}\frac{\xi_{j,\mathbf{k}}}{\omega_n^2+\xi_{j,\mathbf{k}}^2}\right]\\ &= 2\pi\mathcal{V}\sum_{j=1}^{2}\rho_{j,0}\left\langle\frac{1}{1+e^{\xi/T_c}}\right\rangle_j^{\Lambda},\end{aligned} \tag{12}$$

where $\mathcal{V}$ denotes the total volume of the system (or total area, in the 2D case). Note that, here, the upper integration cutoff is the bandwidth Λ.

The numerical solution of Eqs. (9) and (12) are straightforward, and gives $T_c(N)$ as shown in Figs. 2(a) and 2(b) for the 2D and 3D cases, respectively. In these figures, T_c is normalized by ε_0 and N is normalized by the critical value N_c at which the LT takes place, which corresponds to $\mu(0)=\varepsilon_0$. For this particular figure, we used the same density of states for both bands ($\rho_{1,0}=\rho_{2,0}$), we set the interaction cutoff and the bandwidth to the same value $\Omega_0=\Lambda=5\varepsilon_0$, and considered dominant intraband interactions $\lambda_{11}=\lambda_{22}=0.13$ with subleading interband interactions, $|\lambda_{12}|\ll\lambda_{11}$. The main feature is the enhancement of T_c in the vicinity of the LT. Such an enhancement is sharper for 2D bands since in this case the density of states is discontinuous as the chemical potential crosses the band edge.

B. Asymptotic solution

To set the stage for the analytic investigations of the dirty case, here we derive an analytic asymptotic expression for $T_c(\mu)$ in the particular case of 2D bands. Note that, as discussed in Ref. [39] and illustrated in Fig. 2, the case of 3D bands is qualitatively similar than the 2D case. The main quantitative differences arise from the fact that the density of states of the 3D bands vanish smoothly at the band edge. Moreover, because the behavior of the curves $T_c(\mu)$ and $T_c(N)$ are very similar, as illustrated in Fig. 2(c), we will focus on the former.

Returning to the matrix elements $(\hat{A}_{\text{clean}})_{ij}$ in Eq. (10), it is clear that the main effect of the LT is on the lower integration limits W_i. Recall that $W_1=-\mu$ is the bottom of band 1 and $W_2=-\mu+\varepsilon_0$ is the bottom of band 2. If the chemical potential was such that $\mu\gg\Omega_0$, the problem would be in the high-density limit, and we would recover the usual BCS result $(\hat{A}_{\text{clean}})_{ij} = \delta_{ij}(\frac{\rho_{i,F}}{\rho_{i,0}})\ln(\frac{1.13\Omega_0}{T_c})$, where $\rho_{i,F}$ is the density of states at the Fermi level. To capture the behavior near the LT, we first perform the energy integration and obtain

$$(\hat{A}_{\text{clean}})_{ii} = T_c\sum_n\frac{1}{\omega_n}\left[\arctan\left(\frac{\Omega_0}{\omega_n}\right) - \arctan\left(\frac{W_i}{\omega_n}\right)\right]. \tag{13}$$

For each band, there are two different asymptotic regimes in which the Matsubara sum can be evaluated analytically: $|W_i|\ll T_c$ and $|W_i|\gg T_c$ (note that, in our weak-coupling approach, $\Omega_0\gg T_c$ always). This defines four regions in the (μ,T_c) phase diagram, as schematically shown in Fig. 3:

(1) In region I, we have $-W_1<T_c$ and $W_2>T_c$. This region corresponds to $\mu<\mu_1^*$, with $\mu_1^*\sim T_c(\mu_1^*)$.

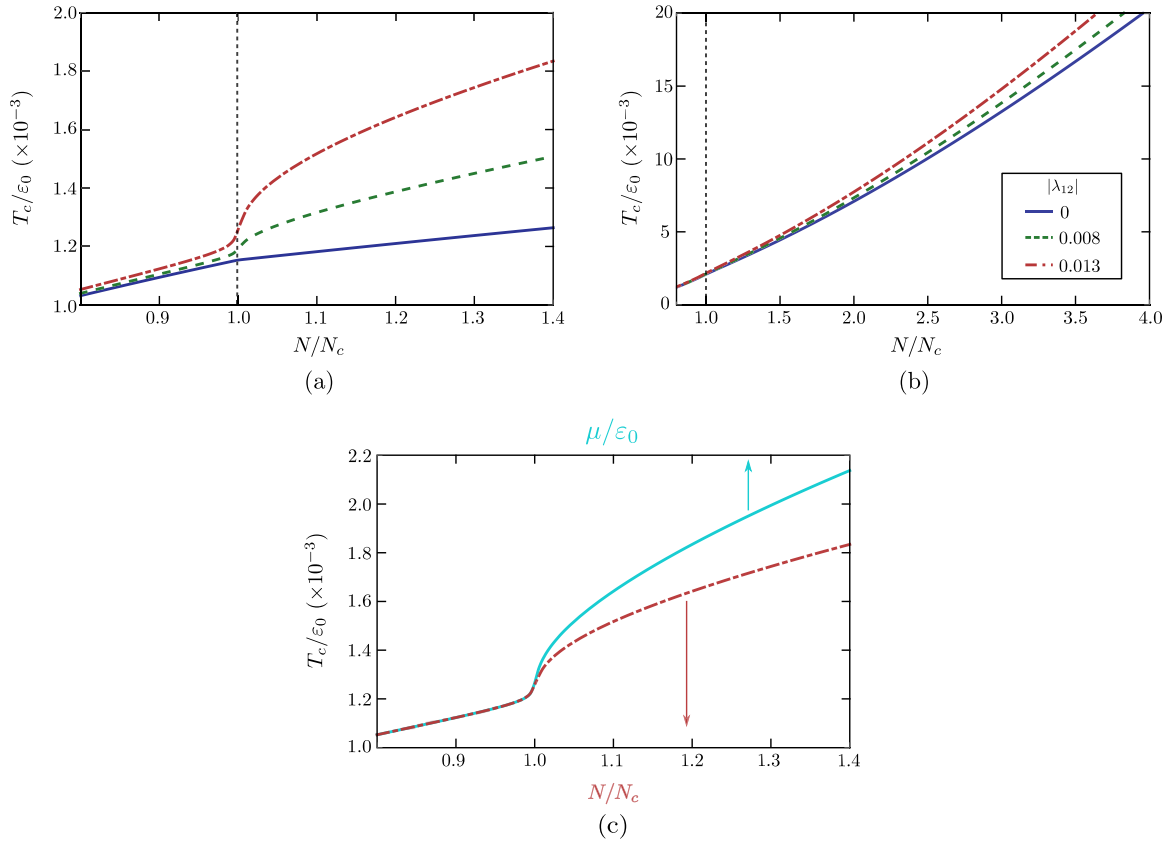

FIG. 2. Phase diagram of the clean two-band SC: the first two panels show T_c as function of the occupation number N for (a) 2D bands and (b) 3D bands, for several values of the parameter λ_{12}. In panel (c), we compare T_c as a function of N with T_c as a function of the chemical potential $\mu(T_c)$ for the 2D case with $|\lambda_{12}| = 0.013$. In all panels, $\lambda_{11} = \lambda_{22} = 0.13$ and $\rho_{2,0} = \rho_{1,0}$. Note that T_c is normalized by the energy displacement between the bands ε_0 and N is normalized by the critical occupation number N_c at which the LT takes place.

(2) In region II, we have $-W_1 > T_c$ and $W_2 > T_c$. This region corresponds to $\mu_1^* < \mu < \mu_2^*$, with $\mu_2^* \sim \varepsilon_0 - T_c(\mu_2^*)$.

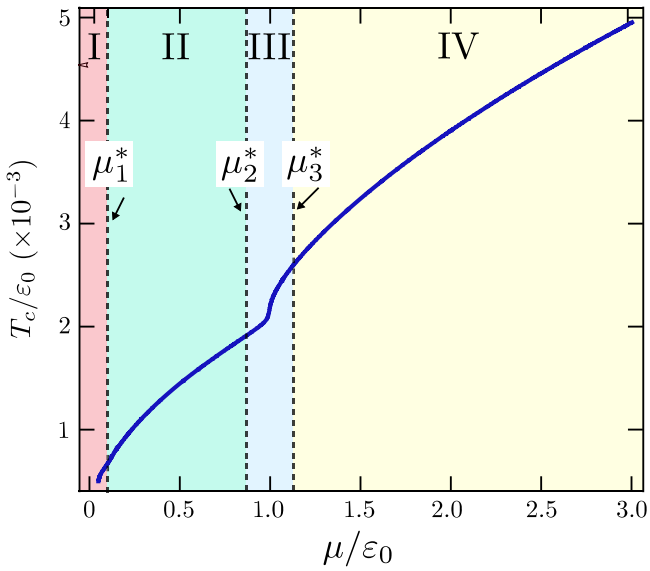

FIG. 3. Regions of the (μ,T) phase diagram for the calculation of the asymptotic behavior of $T_c(\mu)$ in the clean and dirty regimes. The size of the regions are exaggerated for schematic purposes. The precise definition of each region is given in the main text.

(3) In region III, we have $-W_1 > T_c$ and $|W_2| < T_c$. This region corresponds to $\mu_2^* < \mu < \mu_3^*$, with $\mu_3^* \sim \varepsilon_0 + T_c(\mu_3^*)$.

(4) In region IV, we have $-W_1 > T_c$ and $-W_2 > T_c$. This region corresponds to $\mu > \mu_3^*$.

As shown in Appendix A, we find the diagonal matrix elements in each region:

$$(\hat{A}_{\text{clean}})_{11} \sim \frac{1}{2}\begin{cases} \ln\left(\frac{\kappa\Omega_0}{T_c}\right) + \frac{\mu}{2T_c}, & \text{region I} \\ \ln\left(\frac{\kappa^2\Omega_0\mu}{T_c^2}\right), & \text{otherwise} \end{cases}, \tag{14}$$

and

$$(\hat{A}_{\text{clean}})_{22} \sim \frac{1}{2}\begin{cases} \ln\left(\frac{\Omega_0}{\varepsilon_0-\mu}\right), & \text{regions I and II} \\ \ln\left(\frac{\kappa\Omega_0}{T_c}\right) + \frac{(\mu-\varepsilon_0)}{2T_c}, & \text{region III} \\ \ln\left(\frac{\kappa^2\Omega_0(\mu-\varepsilon_0)}{T_c^2}\right), & \text{region IV} \end{cases}, \tag{15}$$

where $\kappa = 2e^{\gamma}/\pi \approx 1.13$, with γ denoting Euler's constant. Solving the gap Eq. (11) now corresponds to solving a simple transcendental equation, since $(\hat{A}_{\text{clean}})_{11}$ and $(\hat{A}_{\text{clean}})_{22}$ are analytic functions of μ and T_c. This is in contrast to the full numerical solution, which requires numerical evaluation of Matsubara sums or energy integrations.

In Fig. 4(a), we compare the asymptotic and numerical results for the 2D clean system, demonstrating their excellent

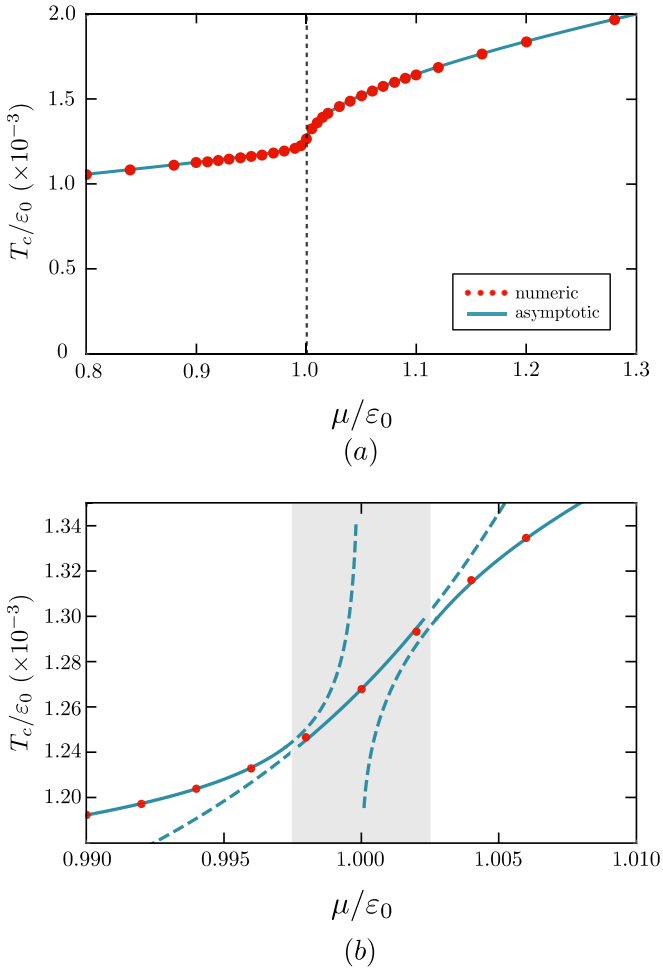

FIG. 4. Comparison between the numerical (symbols) and asymptotic analytical results (solid curve) for T_c, as function of the chemical potential μ, for the 2D clean system across the Lifshitz transition at $\mu = \varepsilon_0$. Panel (b) is a zoom of panel (a) that highlights the very narrow range of μ for which the asymptotic solutions start to fail (gray dashed area). The parameters used here are the same as in Fig. 2(c).

agreement. It is important to emphasize that, due to its very nature, the asymptotic solution is not continuous across the boundaries defining the different regions. In fact, as shown in Fig. 4(b), some of the asymptotic solutions show diverging behavior near the boundaries. Importantly, as highlighted in the same figure, the ranges of μ for which the asymptotic solutions do not behave well are very small—in fact, they are too small to be shown in the scale of Fig. 4(a), and are thus omitted in that plot. Although, in the clean case, the advantages of the asymptotic approach may seem rather minor, it will play an important role in gaining insight to the behavior of the dirty system.

III. DIRTY TWO-BAND SUPERCONDUCTOR

The effects of impurities in our model are captured by adding to Eq. (3) the impurity Hamiltonian

$$H_{\rm imp} = \sum_{\mathbf{k},\mathbf{k}',\sigma} \sum_{\alpha,\beta} W_{\alpha\beta}(\mathbf{k}-\mathbf{k}') c^{\dagger}_{\alpha,\mathbf{k}\sigma} c_{\beta,\mathbf{k}'\sigma}, \tag{16}$$

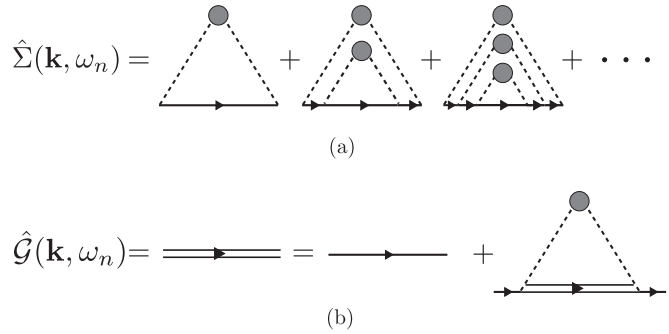

FIG. 5. Panel (a) shows the diagrammatic expansion for the self-energy in the self-consistent Born approximation. Panel (b) shows the Dyson's equation for the total Green's function according to the self-consistent Born approximation. The solid single lines represent $\hat{\mathcal{G}}_0(\mathbf{k},\omega_n)$, while the dashed lines refer to the impurity potential $\hat{W}_{\mathbf{k},\mathbf{k}'}$.

where $W_{\alpha\beta}(\mathbf{q})$ is the impurity potential. Because we are interested in the case of incipient bands, we focus on small-momentum impurity scattering. For simplicity, we consider equal intraband impurity potential, $v \equiv W_{11}(0) = W_{22}(0)$, and interband impurity potential $u \equiv W_{12}(0) = W_{21}(0)$.

To proceed, we consider the standard self-consistent Born approximation, as illustrated in Fig. 5. The Green's function in Nambu space is given self-consistently by Dyson's equation:

$$\hat{\mathcal{G}}^{-1}(\mathbf{k},\omega_n) = \hat{\mathcal{G}}_0^{-1}(\mathbf{k},\omega_n) - \hat{\Sigma}(\mathbf{k},\omega_n), \tag{17}$$

where the matrix $\hat{\mathcal{G}}_0(\mathbf{k},\omega_n)$ is the Green's function of the clean system shown above in Eq. (4), and $\hat{\Sigma}(\mathbf{k},\omega_n)$ is the impurity self-energy:

$$\hat{\Sigma}(\mathbf{k},\omega_n) = n_{\rm imp} \int \frac{d^d k'}{(2\pi)^d} \hat{W}_{\mathbf{k}'-\mathbf{k}} \hat{\mathcal{G}}(\mathbf{k}',\omega_n) \hat{W}_{\mathbf{k}-\mathbf{k}'}. \tag{18}$$

Here, $n_{\rm imp}$ is the impurity concentration and $\hat{W}_{\mathbf{k},\mathbf{k}'}$ represents the impurity potential in Nambu space,

$$\hat{W}_{\mathbf{k},\mathbf{k}'} = \begin{pmatrix} v & 0 & u & 0 \\ 0 & -v & 0 & -u \\ u & 0 & v & 0 \\ 0 & -u & 0 & -v \end{pmatrix}. \tag{19}$$

$\hat{\mathcal{G}}$ can be parametrized by the same matrix structure as $\hat{\mathcal{G}}_0$ in Eq. (4), but with renormalized Matsubara frequencies $\tilde{\omega}_{n,j}$, energy dispersions $\tilde{\xi}_{j,\mathbf{k}} \equiv \xi_{j,\mathbf{k}} + h_{n,j}$, and SC gaps $\tilde{\Delta}_j$. As a result, we find the following set of self-consistent equations:

$$\tilde{\omega}_{n,i} = \omega_n + \sum_j \frac{\tau_{ij}^{-1}\tilde{\omega}_{n,j}}{2} \left\langle \frac{1}{\tilde{\omega}_{n,j}^2 + (\xi + h_{n,j})^2 + \tilde{\Delta}_j^2} \right\rangle_j^{\Lambda}, \tag{20}$$

$$\tilde{\Delta}_i = \Delta_i + \sum_j \frac{\tau_{ij}^{-1}\tilde{\Delta}_j}{2} \left\langle \frac{1}{\tilde{\omega}_{n,j}^2 + (\xi + h_{n,j})^2 + \tilde{\Delta}_j^2} \right\rangle_j^{\Lambda}, \tag{21}$$

$$h_{n,i} = -\sum_j \frac{\tau_{ij}^{-1}}{2} \left\langle \frac{\xi + h_{n,j}}{\tilde{\omega}_{n,j}^2 + (\xi + h_{n,j})^2 + \tilde{\Delta}_j^2} \right\rangle_j^{\Lambda}, \tag{22}$$

where we introduced the impurity scattering rates $\tau_{ij}^{-1} = 2\pi n_{\rm imp}\rho_{j,0}(|v|^2\delta_{i,j} + |u|^2\delta_{\bar{i},j})$, with $\bar{i} = 1(2)$ if $i = 2(1)$. We

also introduced here the bandwidth Λ, which we set to be the same for both bands, for simplicity. Since we are interested in the linearized gap equation, we can take the limit of $\tilde{\Delta}_i \to 0$ in the equations above. The linear relationship between $\tilde{\Delta}_i$ and Δ_i is then given by

$$\begin{pmatrix}\tilde{\Delta}_1\\ \tilde{\Delta}_2\end{pmatrix} = \frac{1}{D_n}\hat{M}_n\begin{pmatrix}\Delta_1\\ \Delta_2\end{pmatrix}, \tag{23}$$

where the matrix $\hat{M}$ is

$$\begin{aligned}\left(\hat{M}_n\right)_{ij} = &\left(1 - \frac{\tau_{\bar{i}\bar{i}}^{-1}}{2}\left\langle\frac{1}{\tilde{\omega}_{n,\bar{i}}^2 + (\xi + h_{n,\bar{i}})^2}\right\rangle_{\bar{i}}^{\Lambda}\right)\delta_{i,j}\\ &+ \frac{\tau_{ij}^{-1}}{2}\left\langle\frac{1}{\tilde{\omega}_{n,j}^2 + (\xi + h_{n,j})^2}\right\rangle_{j}^{\Lambda}\delta_{\bar{i},j},\end{aligned} \tag{24}$$

and $D_n \equiv \det(\hat{M}_n)$ is its determinant, given explicitly by

$$\begin{aligned}D_n = 1 &- \sum_i \frac{\tau_{ii}^{-1}}{2}\left\langle\frac{1}{\tilde{\omega}_{n,i}^2 + (\xi + h_{n,i})^2}\right\rangle_{i}^{\Lambda}\\ &+ \frac{\det(\hat{\tau}^{-1})}{4}\prod_i\left\langle\frac{1}{\tilde{\omega}_{n,i}^2 + (\xi + h_{n,i})^2}\right\rangle_{i}^{\Lambda},\end{aligned} \tag{25}$$

with $(\hat{\tau}^{-1})_{ij} \equiv \tau_{ij}^{-1}$. To calculate T_c, we once again relate the pair expectation value with the anomalous Green's function, $\langle c_{i,-\mathbf{k}\downarrow}c_{i,\mathbf{k}\uparrow}\rangle = T\sum_n \mathcal{F}_i(\mathbf{k},\omega_n)$. Using the relationship between $\tilde{\Delta}_i$ and Δ_i above, we obtain a gap equation of the same form of Eq. (9), but with the matrix $\hat{A}_{\text{clean}} \to \hat{A}_{\text{dirty}}$. The new matrix is given by

$$(\hat{A}_{\text{dirty}})_{ij} = \pi T_c\sum_n \frac{B_i^{(n)}}{D_n}\left(\delta_{ij} + C_{ij}^{(n)}\right), \tag{26}$$

where

$$B_i^{(n)} = \left\langle\frac{1}{\tilde{\omega}_{n,i}^2 + (\xi + h_{n,i})^2}\right\rangle_{i}^{\Omega_0}, \tag{27}$$

and

$$\begin{aligned}C_{ij}^{(n)} = &-\delta_{i,j}\frac{\tau_{\bar{i}\bar{i}}^{-1}}{2}\left\langle\frac{1}{\tilde{\omega}_{n,\bar{i}}^2 + (\xi + h_{n,\bar{i}})^2}\right\rangle_{\bar{i}}^{\Lambda}\\ &+ \delta_{\bar{i},j}\frac{\tau_{ij}^{-1}}{2}\left\langle\frac{1}{\tilde{\omega}_{n,j}^2 + (\xi + h_{n,j})^2}\right\rangle_{j}^{\Lambda}.\end{aligned} \tag{28}$$

It is clear that, when $\hat{\tau} = 0$, $\hat{A}_{\text{dirty}}$ reduces to $\hat{A}_{\text{clean}}$. Similarly, the equation relating the chemical potential μ to the total number of electrons N is modified to

$$N = 2\sum_{\mathbf{k}}\left[1 - T_c\sum_{j,n}\frac{(\xi_{j,\mathbf{k}} + h_{n,j})}{\tilde{\omega}_{n,j}^2 + (\xi_{j,\mathbf{k}} + h_{n,j})^2}\right]. \tag{29}$$

Solving Eqs. (20) and (22) together with the eigenvalue problem and the number equation, we can determine $T_c(N)$ numerically. The results, which were presented in Ref. [39], reveal a pronounced suppression of T_c at the LT in the case of dominant attractive intraband pairing and subdominant repulsive interband pairing. In the case of subdominant attractive interband pairing, the suppression is much milder. These results are reproduced for completeness in Fig. 6.

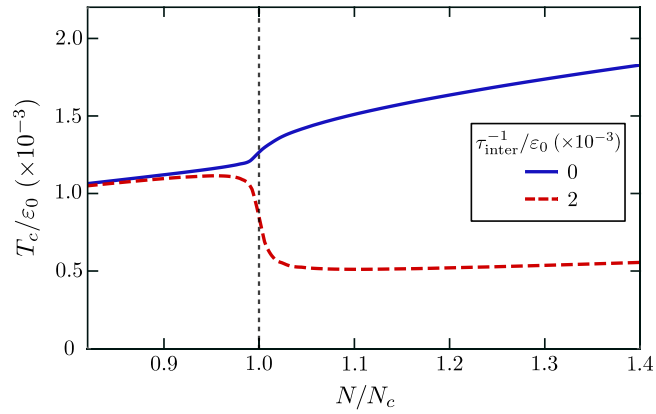

FIG. 6. Superconducting transition temperature T_c as a function of the occupation number N of a dirty two-band SC with 2D bands. The dashed line corresponds to finite interband impurity scattering (dirty system), whereas the solid line corresponds to the clean system. The parameters are the same as in Fig. 2(c); here, the intraband impurity scattering is set to zero.

While Ref. [39] discussed in detail the implications of this numerical result for the understanding of the phase diagrams of $SrTiO_3$ and $LaAlO_3/SrTiO_3$, here we are interested in the mechanisms behind this suppression of T_c near the LT, and its generalization to a wider parameter regime that goes beyond those applicable to the materials above. To achieve this goal, we develop now an analytical asymptotic solution of T_c in two different regimes: the dilute regime and the high-density regime.

IV. ASYMPTOTIC SOLUTION OF THE DIRTY TWO-BAND SUPERCONDUCTOR

Our goal here is to analytically study $T_c(\hat{\tau}^{-1})$ in the different regions of the two-band superconductor (μ, T_c) phase diagram shown in Fig. 3. To avoid cumbersome notations, we denote $T_c(\hat{\tau}^{-1} = 0) \equiv T_{c,0}$, and $\hat{A}_{\text{dirty}} \equiv \hat{A}_d$, $\hat{A}_{\text{clean}} = \hat{A}_c$. Since the general function for $T_c(\hat{\tau}^{-1})$ has no analytic form, we will focus here on the behavior for weak disorder and compute $\partial T_c/\partial\tau_{ij}^{-1}$. This quantity can be conveniently calculated applying Hellmann-Feynman theorem (see, for instance, Refs. [40,41]). Recall that T_c is given by the solution of the linearized gap equation $\hat{\Delta} = (\hat{\lambda}\hat{A}_d)\hat{\Delta}$. Let $\alpha(T)$ be the largest eigenvalue of $(\hat{\lambda}\hat{A}_d)$ for a given temperature T and $\alpha_0(T)$ the largest eigenvalue of $(\hat{\lambda}\hat{A}_c)$. Denote by $\langle\alpha_L^{(0)}|$ and $|\alpha_R^{(0)}\rangle$ the left and right eigenvectors corresponding to $\alpha_0(T)$. Hellmann-Feynman theorem states that

$$\left.\frac{\partial\alpha}{\partial\tau_{ij}^{-1}}\right|_{\tau_{ij}^{-1}=0} = \frac{\left\langle\alpha_L^{(0)}\right|\frac{\partial(\hat{\lambda}\hat{A}_d)}{\partial\tau_{ij}^{-1}}\left|\alpha_R^{(0)}\right\rangle}{\left\langle\alpha_L^{(0)}\middle|\alpha_R^{(0)}\right\rangle}. \tag{30}$$

Note that, because $\hat{\lambda}\hat{A}_d$ is generally nonsymmetric, we need to introduce both left and right eigenvectors. Recall that we focus here on the case of fixed chemical potential μ. Since

$\alpha(T_c) = 1$, using Maxwell relations, we obtain [40,41]

$$\left.\frac{\partial T_c}{\partial \tau_{ij}^{-1}}\right|_{\tau_{ij}^{-1}=0} = -\frac{\langle \alpha_L^{(0)} | \frac{\partial(\hat{\lambda}\hat{A}_d)}{\partial \tau_{ij}^{-1}} | \alpha_R^{(0)} \rangle}{\langle \alpha_L^{(0)} | \alpha_R^{(0)} \rangle} \frac{1}{(\partial\alpha_0/\partial T)|_{T=T_c}}. \quad (31)$$

Our goal here is to compare the changes in T_c promoted by impurity scattering in the high-density and dilute regimes.

A. High-density regime

We first discuss the high-density regime, i.e., when the system is far from the LT, and the chemical potential is away from the band edge, $\mu \gg \{\Omega_0, \varepsilon_0\}$. This is the parameter regime most commonly studied in BCS-type approaches to two-band superconductivity. We will recover here several results previously published in the literature [18,42,43], but also set the stage for the analysis near the LT.

Because $\mu \gg \{\Omega_0, \varepsilon_0\}$, the lower cutoff of the energy integrals Eq. (8) is modified according to

$$\langle \mathcal{O}(\xi) \rangle_i^{\xi_c} \equiv \frac{\rho_{i,F}}{\pi \rho_{i,0}} \int_{-\xi_c}^{\xi_c} d\xi \, \mathcal{O}(\xi), \quad (32)$$

where ξ_c can assume the values Ω_0 or Λ, and we replaced the density of states by its value at the Fermi level, $\rho_{i,F} \equiv \rho_i(\xi_F)$. In this regime, we can also neglect the renormalization $h_{n,i}$ of the band dispersions. The integrals that appear in the definitions of $\tilde{\omega}_n$ and $\hat{A}_d$ can then be computed in a straightforward way:

$$\left\langle \frac{1}{\tilde{\omega}_{n,i}^2 + \xi^2} \right\rangle_i^{\Omega_0} = \left\langle \frac{1}{\tilde{\omega}_{n,i}^2 + \xi^2} \right\rangle_i^{\Lambda} = \frac{\rho_{i,F}}{\rho_{i,0}|\tilde{\omega}_{n,i}|}. \quad (33)$$

As a result, the self-consistent equation for $\tilde{\omega}_{n,i}$ can be solved analytically, yielding

$$|\tilde{\omega}_{n,i}| = |\omega_n| + \frac{1}{2}\sum_j \tau_{ij}^{-1}. \quad (34)$$

In the expression above and in the remainder of this section, we renormalize the scattering rates and coupling constants such that $\frac{\rho_{i,F}}{\rho_{i,0}} \tau_{ij}^{-1} \to \tau_{ij}^{-1}$ and $\frac{\rho_{i,F}}{\rho_{i,0}} \lambda_{ij} \to \lambda_{ij}$. This corresponds to using the density of states at the Fermi level $\rho_{i,F}$, instead of $\rho_{i,0}$, in the corresponding definitions, i.e., in this section $\lambda_{ij} = -\rho_{j,F} V_{ij}$ and $\tau_{ij}^{-1} = 2\pi n_{\rm imp} \rho_{j,F}(|v|^2 \delta_{i,j} + |u|^2 \delta_{\bar{i},j})$.

Thus, the different components of $(\hat{A}_d)_{ij} = \pi T_c \sum_n \frac{B_i^{(n)}}{D_n}(\delta_{ij} + C_{ij}^{(n)})$ become

$$\frac{B_i^{(n)}}{D_n} = \frac{\left(|\omega_n| + \frac{1}{2}\sum_j \tau_{\bar{i}j}^{-1}\right)}{|\omega_n|\left(|\omega_n| + \frac{1}{2}\sum_j \tau_{j\bar{j}}^{-1}\right)}, \quad (35)$$

$$\frac{B_i^{(n)}}{D_n} C_{ij}^{(n)} = \frac{\left(-\delta_{i,j}\tau_{\bar{i}\bar{i}}^{-1} + \delta_{\bar{i},j}\tau_{i\bar{i}}^{-1}\right)}{2|\omega_n|\left(|\omega_n| + \frac{1}{2}\sum_j \tau_{j\bar{j}}^{-1}\right)}, \quad (36)$$

where

$$D_n = \frac{|\omega_n|\left(|\omega_n| + \frac{1}{2}\sum_j \tau_{j\bar{j}}^{-1}\right)}{\prod_i \left(|\omega_n| + \frac{1}{2}\sum_j \tau_{ij}^{-1}\right)}. \quad (37)$$

The Matsubara sums appearing in $\hat{A}_d$ can be evaluated using the result

$$\sum_n \frac{1}{|\omega_n| + x} \approx \frac{1}{\pi T_c}\left[\ln\left(\frac{\Gamma_c}{2\pi T_c}\right) - \psi\left(\frac{1}{2} + \frac{x}{2\pi T_c}\right)\right], \quad (38)$$

where Γ_c is the upper cutoff of the Matsubara sum (which is $\Gamma_c = \Omega_0 \gg T_c$ for the $B_i^{(n)}$ terms), and $\psi(x)$ is the digamma function. We find that $\hat{A}_d$ can be cast in the form

$$(\hat{A}_d)_{ij} = \delta_{i,j} P_i + \delta_{\bar{i},j} Q_i, \quad (39)$$

with

$$P_i = \ln\left(\frac{\kappa\Omega_0}{T_c}\right) - \frac{\rho_{\bar{i},F}}{\rho_{1,F} + \rho_{2,F}}\left[\psi\left(\frac{1}{2} + \frac{\tau_{\rm inter}^{-1}}{2\pi T_c}\right) - \psi\left(\frac{1}{2}\right)\right], \quad (40)$$

$$Q_i = \frac{\rho_{\bar{i},F}}{\rho_{1,F} + \rho_{2,F}}\left[\psi\left(\frac{1}{2} + \frac{\tau_{\rm inter}^{-1}}{2\pi T_c}\right) - \psi\left(\frac{1}{2}\right)\right], \quad (41)$$

where $\tau_{\rm inter}^{-1} \equiv \frac{1}{2}(\tau_{12}^{-1} + \tau_{21}^{-1})$ is the average interband impurity scattering and $\kappa \approx 1.13$ is the same constant that appears in Sec. II for the clean case.

It is clear that $\hat{A}_d$ depends only on the average interband impurity scattering $\tau_{\rm inter}^{-1}$, i.e., T_c is unaffected by intraband impurity scattering. This is not surprising, since the gaps are isotropic and Anderson's theorem enforces that intraband nonmagnetic impurity scattering cannot affect superconductivity. Using these expressions, the solution of the gap equations, corresponding to finding the largest eigenvalue of $(\hat{\lambda}\hat{A}_d)$, becomes a transcendental equation that can be solved in a straightforward way.

We now proceed to evaluate $\partial T_c/\partial \tau_{\rm inter}^{-1}$ using Eq. (31). For convenience, we introduce the ratio between the densities of states of the two bands to be $r \equiv \rho_{2,F}/\rho_{1,F}$. By definition, it follows that $\lambda_{12}/\lambda_{21} = \tau_{12}^{-1}/\tau_{21}^{-1} = r$. The largest eigenvalue of the clean gap equation is given by

$$\alpha_0 = \lambda_+ \ln\left(\frac{\kappa\Omega_0}{T_c}\right), \quad (42)$$

where

$$\lambda_+ = \lambda_0 + \sqrt{\delta\lambda^2 + \frac{1}{r}\lambda_{12}^2}. \quad (43)$$

For simplicity of notation, here we introduced $\lambda_0 = \frac{1}{2}(\lambda_{11} + \lambda_{22})$ and $\delta\lambda = \frac{1}{2}(\lambda_{11} - \lambda_{22})$. The right and left eigenvectors are given by

$$|\alpha_R^{(0)}\rangle = \begin{pmatrix} \delta\lambda + \sqrt{\delta\lambda^2 + \frac{1}{r}\lambda_{12}^2} \\ \frac{1}{r}\lambda_{12} \end{pmatrix}, \quad (44)$$

and

$$\langle \alpha_L^{(0)}| = \begin{pmatrix} \delta\lambda + \sqrt{\delta\lambda^2 + \frac{1}{r}\lambda_{12}^2} \\ \lambda_{12} \end{pmatrix}^T. \quad (45)$$

Note that the relative sign of the two components of the eigenvectors, which correspond to the ratio between the two gaps Δ_1/Δ_2, is determined solely by $\mathrm{sgn}(\lambda_{12}) = \mathrm{sgn}(\lambda_{21})$, i.e.,

$\mathrm{sgn}(\Delta_1/\Delta_2) = \mathrm{sgn}(\lambda_{12})$. As explained in Sec. II, this implies that attractive interband pairing interaction, $\lambda_{12} > 0$, promotes a sign-preserving s^{++} state, whereas repulsive interband pairing interaction, $\lambda_{12} < 0$, promotes a sign-changing s^{+-} state.

Next, from the definition of $\hat{A}_d$ in Eq. (39), we obtain

$$\left.\frac{\partial(\hat{\lambda}\hat{A}_d)}{\partial\tau_{\mathrm{inter}}^{-1}}\right|_{\tau_{\mathrm{inter}}^{-1}=0} = \frac{1}{(1+r)}\frac{\pi}{4T_{c,0}} \times \begin{pmatrix} \lambda_{12}-r\lambda_{11} & -\lambda_{12}+r\lambda_{11} \\ \lambda_{22}-\lambda_{12} & -\lambda_{22}+\lambda_{12} \end{pmatrix} \quad (46)$$

It is straightforward to now compute $\partial T_c/\partial\tau_{\mathrm{inter}}^{-1}$ via Eq. (31), using that $\frac{\partial\alpha_0}{\partial T_c} = -\frac{\lambda_+}{T_{c,0}}$. The full expression is long and not very insightful. In the particular case of $r = 1$, however, the expression simplifies significantly and we obtain

$$\left.\frac{\partial T_c}{\partial\tau_{\mathrm{inter}}^{-1}}\right|_{\tau_{\mathrm{inter}}^{-1}=0} = -\frac{\pi}{8}\left[1 - \frac{\mathrm{sgn}(\lambda_{12})}{\sqrt{\left(\frac{\lambda_{11}-\lambda_{22}}{2\lambda_{12}}\right)^2+1}}\right]. \quad (47)$$

This expression reveals important properties of impurity scattering in multiband SC. First, as mentioned above, only interband impurity scattering is pair-breaking. Second, this pair-breaking effect takes place generically for both s^{+-} and s^{++} states. Indeed, as long as $\lambda_{11} \neq \lambda_{22}$, T_c will be suppressed by impurities regardless of the sign of the interband interaction λ_{12}.

It is clear, however, that the suppression is stronger in the case of repulsive interaction $\lambda_{12} < 0$. Compared to the Abrikosov-Gor'kov result for the suppression rate of T_c by magnetic impurity scattering in single-band s-wave SC, $\left(\frac{\partial T_c}{\partial\tau_{\mathrm{mag}}^{-1}}\right)_{\mathrm{AG}} = -\frac{\pi}{4}$, it follows that $\left|\frac{\partial T_c}{\partial\tau_{\mathrm{inter}}^{-1}}\right| \leqslant \left|\frac{\partial T_c}{\partial\tau_{\mathrm{mag}}^{-1}}\right|$. Note that, according to the expression for the leading eigenvector Eq. (44), the magnitudes of the two gaps are necessarily different when $\lambda_{11} \neq \lambda_{22}$, i.e., $|\Delta_1| \neq |\Delta_2|$. In the fine-tuned case of equal intraband pairing interactions, $\lambda_{11} = \lambda_{22}$, which corresponds to two gaps of same magnitudes, $|\Delta_1| = |\Delta_2|$, T_c for the s^{++} state displays no suppression with disorder $\tau_{\mathrm{inter}}^{-1}$, whereas T_c for the s^{+-} state displays its maximum suppression. Thus, at the same time that $\lambda_{11} \neq \lambda_{22}$ promotes pair-breaking effects for the s^{++} state, it reduces the pair-breaking effects for the s^{+-} state. This is illustrated in Fig. 7(a).

The difference in the density of states between the two bands, signaled here by $r \neq 1$, plays a similar role as the difference in the intraband pairing interactions. For instance, if we set $\lambda_{11} = \lambda_{22}$ but consider an arbitrary r, we find

$$\left.\frac{\partial T_c}{\partial\tau_{\mathrm{inter}}^{-1}}\right|_{\tau_{\mathrm{inter}}^{-1}=0} = -\frac{\pi}{8}\left[1 - \frac{2\sqrt{r}\,\mathrm{sgn}(\lambda_{12})}{1+r}\right]. \quad (48)$$

Once again, the suppression of T_c for the s^{++} state is minimum (in fact, zero) when $r = 1$, whereas the suppression of T_c for the s^{+-} state is maximum (and equal to the Abrikosov-Gor'kov value) when $r = 1$. This behavior is shown in Fig. 7(b). We emphasize that our analysis reproduces similar conclusions about the role of impurities in multiband SC that have been previously reported elsewhere [18,42,43].

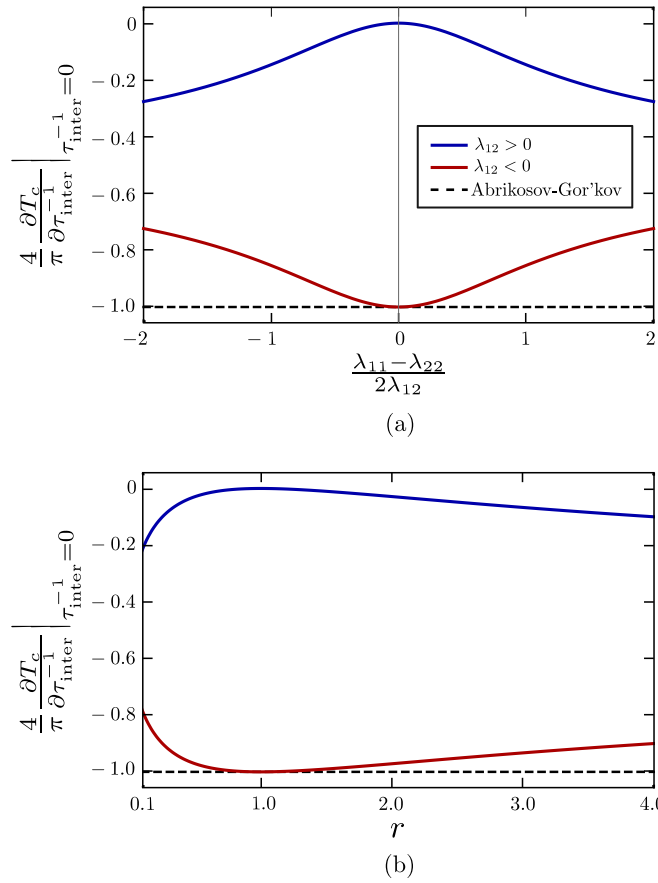

FIG. 7. The rate of suppression of T_c by interband nonmagnetic impurity scattering $\tau_{\mathrm{inter}}^{-1}$, $\frac{\partial T_c}{\partial\tau_{\mathrm{inter}}^{-1}}|_{\tau_{\mathrm{inter}}^{-1}=0}$ for repulsive ($\lambda_{12} < 0$, red curves) and attractive ($\lambda_{12} > 0$, blue curves) interband pairing interactions, in the high-density regime. In panel (a), the density of states of the two bands are set to be the same, but the intraband pairing interactions of the two bands, λ_{11} and λ_{22}, are allowed to be different. In panel (b), λ_{11} is set to be the same as λ_{22}, but the two density of states are allowed to be different, with $r = \rho_{2,F}/\rho_{1,F}$. In both panels, the suppression rates are normalized by the magnitude of the Abrikosov-Gor'kov value of $-\pi/4$, corresponding to the suppression rate of T_c of a single-band superconductor by magnetic impurity scattering.

B. Dilute regime

Our analysis of the high-density regime reveals that impurity pair-breaking effects on T_c arise from the interband scattering rates, τ_{21}^{-1} and τ_{12}^{-1}. Thus, in this subsection, to simplify the analysis, we neglect intraband scattering processes, and set $\tau_{11}^{-1} = \tau_{22}^{-1} = 0$. Furthermore, in the same spirit of the previous subsection, we focus on the weak-disorder regime, in which τ_{12}^{-1} and τ_{21}^{-1} are small compared to $T_{c,0}$. Finally, we consider 2D bands, in which case the density of states does not depend on the energy. Within these approximations, to linear order in the scattering rates, the renormalized Matsubara frequency in Eq. (20) becomes:

$$\tilde{\omega}_{n,i} = \omega_n\left(1 + \frac{1}{2\pi}\tau_{i\bar{i}}^{-1} f_{n,\bar{i}}\right), \quad (49)$$

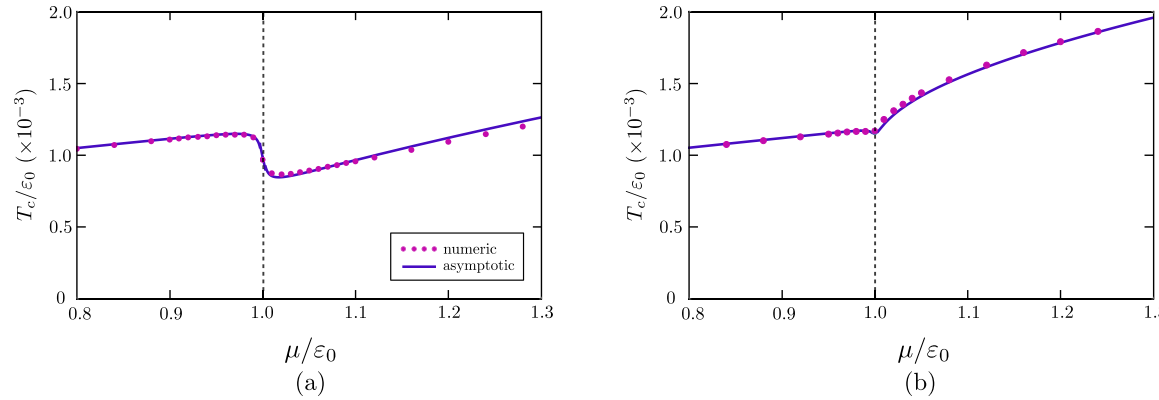

FIG. 8. Comparison between the numerical (symbols) and asymptotic analytical results (solid curves) for T_c, as function of the chemical potential μ, for the 2D dirty system across the Lifshitz transition at $\mu = \varepsilon_0$. The parameters are the same as in Fig. 4 but with $\lambda_{12} < 0$ (repulsive interband pairing interaction) in panel (a) and $\lambda_{12} > 0$ (attractive interband pairing interaction) in panel (b). The interband impurity scattering τ_{inter}^{-1} is set to $\tau_{\text{inter}}^{-1}/\varepsilon_0 = 10^{-3}$.

where we defined the function

$$f_{n,i} \equiv \frac{1}{\omega_n}\left[\arctan\left(\frac{\Omega_0}{\omega_n}\right) - \arctan\left(\frac{W_i}{\omega_n}\right)\right]. \tag{50}$$

Note that, similar to the previous section, we neglect the renormalization of the band due to disorder, $h_{n,i}$. As shown below, this approximation yields very good agreement between the numerical and the asymptotic results. Evaluating the matrix elements of $\hat{A}_d$ in Eq. (26), we find, to linear order in the impurity scattering rate

$$\hat{A}_d = \hat{A}_c + \tau_{\text{inter}}^{-1}\delta\hat{A}. \tag{51}$$

Here, $\hat{A}_c$ is the clean-case diagonal matrix discussed in Sec. II B, $\tau_{\text{inter}}^{-1} \equiv \frac{1}{2}(\tau_{12}^{-1} + \tau_{21}^{-1})$ is the average interband impurity scattering, and $\delta\hat{A}$ is given by

$$(\delta\hat{A})_{ij} = \frac{1}{2\pi}[R_i\delta_{ij} + S(-\delta_{i,j} + \delta_{\bar{i},j})], \tag{52}$$

with

$$R_i = -T_c\sum_n\left(\frac{\Lambda}{\Lambda^2+\omega_n^2} - \frac{W_i}{W_i^2+\omega_n^2}\right)f_{n,\bar{i}},$$

$$S = T_c\sum_n f_{n,1}f_{n,2}. \tag{53}$$

The expressions above are obtained after two simplifications: We set the density of states of the two bands to be equal, $\rho_{1,0} = \rho_{2,0}$, and consider $\Omega_0 = \Lambda$. Note that the main results presented here do not rely on these simplifications.

To determine analytic asymptotic expressions for the matrix elements of $\hat{A}_d$, we follow the same procedure as in the clean case as outlined in Sec. II B, and divide the (μ, T_c) phase diagram in four regions. The calculation is tedious but straightforward; the resulting expressions for R_1, R_2, and S are long and shown explicitly in Appendix B. In terms of these expressions, finding T_c corresponds to solving the transcendental algebraic equation that comes from the condition that the largest eigenvalue of $\hat{\lambda}\hat{A}_d$ equals one (see Appendix C).

In Fig. 8, we compare the numerical and asymptotic analytical results for the cases of attractive and repulsive interband pairing interaction. As in the clean case, the agreement between the two methods is excellent, except in very narrow regions where the asymptotic approximation fails. As in Fig. 4, these regions are too narrow compared to the scale of the plots and are thus not shown in the plots. We note that the agreement between the asymptotic solution and the numerical results near the LT improves as the scattering rates become smaller.

In Figs. 9(a) and 9(b), we plot the analytic asymptotic behavior of $\frac{\partial T_c}{\partial \tau_{\text{inter}}^{-1}}|_{\tau_{\text{inter}}^{-1}=0}$ as function of the chemical potential for attractive and repulsive interband pairing interactions, respectively. Note that the computation of such suppression rate of T_c from Eq. (31) is straightforward and details are provided in Appendix C. Similar to Fig. 7, we normalize $\partial T_c/\partial\tau_{\text{inter}}^{-1}$ by the Abrikosov-Gor'kov suppression rate $-\pi/4$. The insets display zooms of the behaviors of the asymptotic solutions near the LT—as in the analysis of previous sections, the asymptotic solutions are not continuous across the boundaries of the different regions of Fig. 3.

The results far from the LT are not surprising: before the LT, when only one band is present, $\partial T_c/\partial\tau_{\text{inter}}^{-1}$ is very small, since the second band is sunk below the Fermi level. After the LT, when the second band is no longer incipient, $\partial T_c/\partial\tau_{\text{inter}}^{-1}$ approaches the high-density values $-\pi/4$ for repulsive interband interaction and 0 for attractive interband pairing interaction.

The interesting behaviors of $\partial T_c/\partial\tau_{\text{inter}}^{-1}$ take place in the vicinity of the LT. For $\lambda_{12} < 0$, we note a very rapid increase of the magnitude of the suppression rate, despite the fact that the second band is only incipient. On the other hand, for $\lambda_{12} > 0$, the magnitude of the suppression rate displays a rather mild maximum when the second band crosses the Fermi level.

The fate of the evolution of T_c in the dirty system across the LT depends then on the competition between two opposite effects: the suppression of T_c due to the pair-breaking promoted by interband impurity scattering, and the enhancement of T_c promoted by the new electronic states that become part of the superconducting state once the second band crosses the Fermi

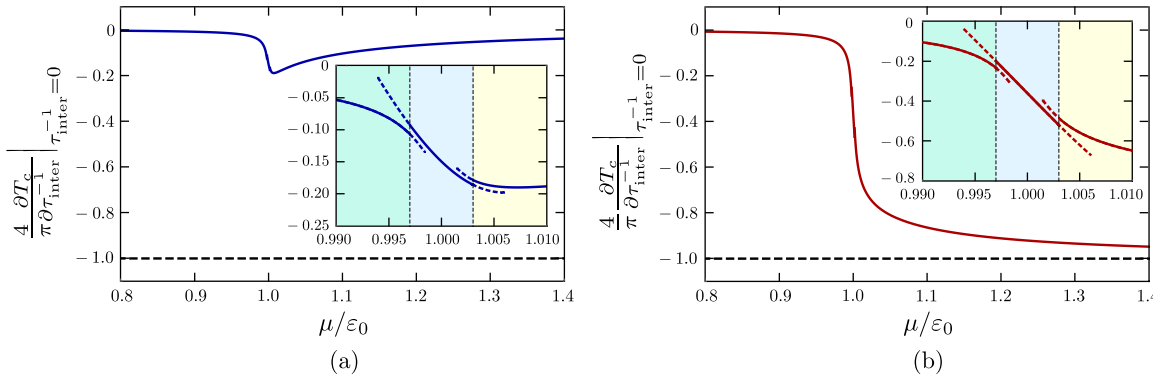

FIG. 9. The rate of suppression of T_c by interband impurity scattering, $\frac{\partial T_c}{\partial \tau_{\rm inter}^{-1}}|_{\tau_{\rm inter}^{-1}=0}$ for attractive [$\lambda_{12} > 0$, panel (a)] and repulsive [$\lambda_{12} < 0$, panel (b)] interband pairing interactions, in the dilute regime. The insets highlight the asymptotic behaviors across the boundaries of regions II, III, and IV of Fig. 3. In both panels, the suppression rates are normalized by the absolute value of the Abrikosov-Gor'kov suppression rate of $-\pi/4$, corresponding to the case of a single-band superconductor by magnetic impurity scattering. The parameters used here are $\rho_{1,0} = \rho_{2,0}$, $\lambda_{11} = \lambda_{22}$, and $\lambda_{12} = \lambda_{21}$.

level. The latter effect is illustrated in Fig. 10, where $\partial T_c/\partial\mu$ obtained from the asymptotic analytical solution of the clean system is shown. Generally, one expects that, for sufficient strong disorder, and for a repulsive interband interaction, the former effect wins, such that T_c displays a maximum at the LT. This is indeed what we observed in the full solution of the dirty gap equations shown in Fig. 8.

V. CONCLUDING REMARKS

In summary, in this paper, we developed an asymptotic analytical framework to investigate the behavior of the superconducting transition temperature T_c across a LT in a dirty two-band system. Our systematic study unveiled two competing effects that influence the evolution of T_c. The first effect arises from the fact that the system gains energy via the opening of a superconducting gap in the incipient band, which leads to an enhancement of T_c (see Fig. 10). The second effect arises because, as soon as the second band emerges above the Fermi level and the gap becomes nonnegligible, pair-breaking effects kick in due to interband impurity scattering, resulting in a suppression of T_c. While the first effect is insensitive to the nature of pairing state—i.e., whether it is an s^{++} state resulting from interband attraction or an s^{+-} state resulting from interband repulsion—the second effect is much stronger in the case of repulsive pairing interactions. As a result, for an s^{+-} superconductor with significant impurity scattering, T_c is expected to be maximum at the LT. Therefore, our results offer important benchmarks to assess indirectly from the shape of the superconducting dome whether a multiband superconductor is conventional (i.e., driven by attractive pairing interactions only) or unconventional (i.e., driven by repulsive pairing interactions). Note that, if the impurities were magnetic, impurity scattering would be strongly pair-breaking for both attractive and repulsive interband interactions (see also Ref. [44]). As a result, although an explicit calculation is beyond the scope of this work, one expects a similar behavior of T_c across the LT in both cases.

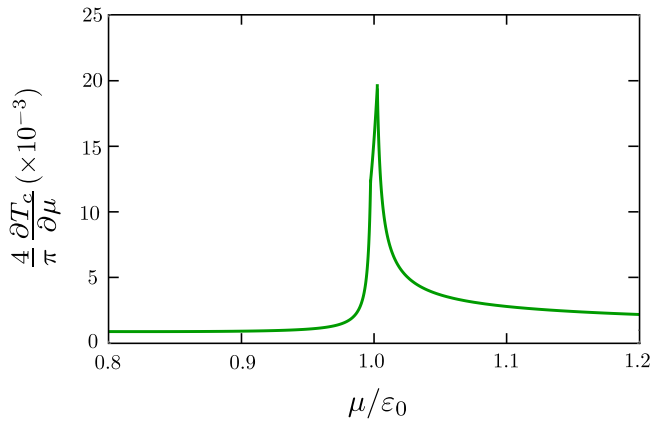

FIG. 10. Rate of enhancement of T_c by changes in the chemical potential, $\frac{\partial T_c}{\partial \mu}$, for the clean 2D system. The parameters are the same as those used in Fig. 9. To make the comparison with that figure more transparent, we also normalize the rate of change of T_c by $\pi/4$.

ACKNOWLEDGMENTS

We thank K. Behnia, A. Chubukov, H. Faria, M. Gastiasoro, G. Lonzarich, and V. Pribiag for fruitful discussions. This work was supported by the U.S. Department of Energy through the University of Minnesota Center for Quantum Materials, under Award No. DE-SC-0016371 (R.M.F.). T.V.T. acknowledges the support from the São Paulo Research Foundation (Fapesp, Brazil) via the BEPE scholarship.

APPENDIX A: MATSUBARA SUMS FOR THE CLEAN CASE

Deriving an analytic expression for the matrix elements $(\hat{A}_{\rm clean})_{ij}$ involves calculating, analytically, Matsubara sums of the type $\sum_n \frac{1}{\omega_n}\arctan(\frac{y}{\omega_n}) = \frac{\text{sign}(y)}{T_c}\, s_1(\frac{|y|}{T_c})$, where the quantity y can assume the values Ω_0, $W_1 = -\mu$ or $W_2 = -\mu + \varepsilon_0$, and

$$s_1(|x|) \equiv 2\sum_{n=0}^{\infty} \frac{1}{(2n+1)\pi}\arctan\left(\frac{|x|}{(2n+1)\pi}\right). \qquad \text{(A1)}$$

We calculate an approximate expression for $s_1(|x|)$, taking advantage of the asymptotic behavior of $\arctan(\frac{|x|}{(2n+1)\pi})$ in two regimes, $|x| \ll 1$ and $|x| \gg 1$. If $|x| \ll 1$, $\frac{|x|}{(2n+1)\pi} \ll 1$ for all n, and a Taylor expansion of $\arctan(\frac{|x|}{(2n+1)\pi})$ leads to

$$s_1(|x| \ll 1) = 2\sum_{l=0}^{\infty} \frac{(-1)^l \zeta(2l+2)[2^{2l+2}-1]}{(2l+1)(2\pi)^{2l+2}} |x|^{2l+1}, \tag{A2}$$

where we used the fact that

$$\sum_{n=0}^{\infty} \frac{1}{[(2n+1)\pi]^k} = \frac{(2^k-1)\zeta(k)}{(2\pi)^k}, \tag{A3}$$

with integer $k \geqslant 2$ and $\zeta(k)$ denoting the Riemann zeta function. The leading term is clearly the $l = 0$:

$$s_1(|x| \ll 1) \sim \frac{|x|}{4}. \tag{A4}$$

On the other hand, if $|x| \gg 1$, $\frac{|x|}{(2n+1)\pi} \gg 1$ for small values of n, but the ratio decreases with increasing n, until it eventually behaves as $\frac{|x|}{(2n+1)\pi} \ll 1$ for large enough n. Denoting by N^* the value of n such that $(2N^*+1)\pi = |x|$, i.e., $N^* = \frac{|x|}{2\pi} - \frac{1}{2}$, we approximate $\arctan(\frac{|x|}{(2n+1)\pi})$ by its Taylor expansion in powers of $1/|x|$ when $0 < n < N^*$, and by its Taylor expansion in powers of $|x|$ when $N^*+1 < n < \infty$. The result is

$$\begin{aligned} s_1(|x| \gg 1) = &\sum_{n=0}^{N^*} \frac{1}{2n+1} \\ &- 2\sum_{l=0}^{\infty} \frac{(-1)^l}{(2l+1)|x|^{2l+1}} \sum_{n=0}^{N^*} [(2n+1)\pi]^{2l} \\ &+ 2\sum_{l=0}^{\infty} \frac{(-1)^l |x|^{2l+1}}{(2l+1)} \sum_{n=N^*+1}^{\infty} \frac{1}{[(2n+1)\pi]^{2l+2}}. \end{aligned} \tag{A5}$$

The sums over n that appear in Eq. (A5) can be evaluated analytically:

$$\sum_{n=0}^{N^*} \frac{1}{[(2n+1)\pi]^k} = \begin{cases} \frac{(2^k-1)\zeta(k)}{(2\pi)^k} + \frac{1}{(2\pi)^k(|k|+1)} B_{|k|+1}\left(1+\frac{|x|}{2\pi}\right), & \text{if } k \leqslant 0 \\ \frac{1}{2\pi}\left[\psi\left(1+\frac{|x|}{2\pi}\right) - \psi\left(\frac{1}{2}\right)\right], & \text{if } k = 1, \\ \frac{(2^k-1)\zeta(k)}{(2\pi)^k} - \frac{1}{(k-1)!}\left(\frac{-1}{2\pi}\right)^k \psi^{(k-1)}\left(1+\frac{|x|}{2\pi}\right), & \text{if } k > 1 \end{cases} \tag{A6}$$

and

$$\sum_{n=N^*+1}^{\infty} \frac{1}{[(2n+1)\pi]^k} = \frac{1}{(k-1)!}\left(\frac{-1}{2\pi}\right)^k \psi^{(k-1)}\left(1+\frac{|x|}{2\pi}\right), \quad \text{if } k \geqslant 2, \tag{A7}$$

where $\psi^{(k)}(x)$, $\psi(x) = \psi^{(0)}(x)$ and $B_k(x)$ are, respectively, the polygamma function of kth order, the digamma function, and the Bernoulli polynomials. In the limit $|x| \gg 1$, a Taylor expansion, up to order $\mathcal{O}(\frac{1}{|x|^k})$ leads to

$$\sum_{n=0}^{N^*} \frac{1}{[(2n+1)\pi]^k} \sim \begin{cases} \frac{1}{2\pi}\ln(\kappa|x|), & \text{if } k = 1 \\ \frac{(2^k-1)\zeta(k)}{(2\pi)^k} - \frac{1}{2\pi(k-1)|x|^{k-1}}, & \text{if } k \leqslant 0 \text{ or } k > 1 \end{cases}, \tag{A8}$$

and

$$\sum_{n=N^*+1}^{\infty} \frac{1}{[(2n+1)\pi]^k} \sim \frac{1}{2\pi(k-1)|x|^{k-1}}, \quad \text{if } k \geqslant 2. \tag{A9}$$

where we defined the constant $\kappa = 2e^{\gamma}/\pi \approx 1.13$, with γ denoting Euler's constant.

Substituting Eqs. (A8) and (A9) into Eq. (A5), we find that its second and third terms result in the same constant $\sum_{l=0}^{\infty} \frac{(-1)^l}{\pi(2l+1)^2} = \frac{\mathcal{C}}{\pi}$ ($\mathcal{C} \approx 0.92$ is the Catalan's constant), differing only by a minus sign. Thus, they cancel out, and we obtain

$$s_1(|x| \gg 1) \sim \tfrac{1}{2}\ln(\kappa|x|). \tag{A10}$$

To summarize, combining Eqs. (A4) and (A10), we have

$$s_1(|x|) \sim \begin{cases} \frac{|x|}{4}, & \text{if } |x| \ll 1 \\ \frac{1}{2}\ln(\kappa|x|), & \text{if } |x| \gg 1 \end{cases}. \tag{A11}$$

Note that $s_1(|x| \to 1^+) \neq s_1(|x| \to 1^-)$. This is because the asymptotic approach we described begins to fail for $|x|$ of order one, as we can see in Fig. 11. As a consequence, the asymptotic expressions for $T_c(\mu)$ deviate from the numeric results when μ approaches the boundaries μ_1^*, μ_2^* and μ_3^* of the regions of the phase diagram illustrated in Fig. 3. At these points, either $|W_1|$ or $|W_2|$ becomes of the order of T_c.

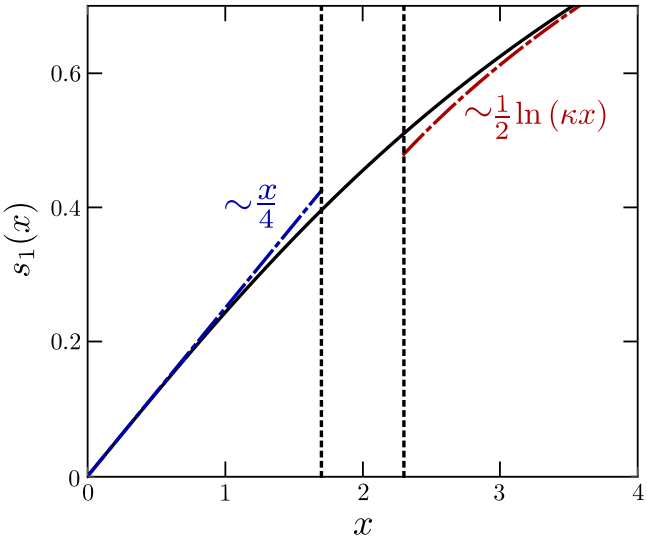

FIG. 11. Numerical and asymptotic solutions for the Matsubara sum Eq. (A1). The dot-dashed blue and red lines are the asymptotic solutions for $|x| \ll 1$ and $|x| \gg 1$, while the solid line is the numerical result. The dashed vertical lines delimit the region where the asymptotic approximation begins to fail.

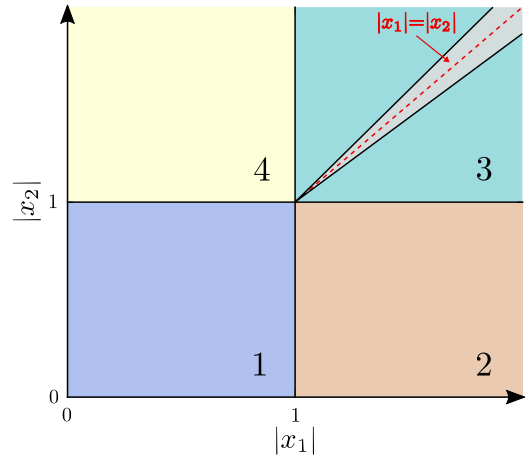

FIG. 12. Different regions of the two-dimensional parameter space $|x_1| \times |x_2|$ in which the analytic expansions are performed. In region 3, the silver area around the line $|x_1| = |x_2|$ indicates the region where the approximations lose precision, since the neglected terms of order $\mathcal{O}(\frac{1}{|x_j|}(\frac{|x_<|}{|x_>|})^2)$, $j = 1,2$, become more important.

APPENDIX B: MATSUBARA SUMS FOR THE DIRTY CASE

In the case of a dirty two-band SC, there are two distinct types of Matsubara sums that we need to calculate for $\delta\hat{A}$, as shown in Eq. (53). The first are sums of the type

$$\sum_n \frac{1}{\omega_n}\arctan\left(\frac{y_1}{\omega_n}\right)\frac{y_2}{y_2^2+\omega_n^2} = \frac{\text{sign}(y_1y_2)}{T_c^2}\, s_2\left(\frac{|y_1|}{T_c},\frac{|y_2|}{T_c}\right), \tag{B1}$$

where we define

$$s_2(|x_1|,|x_2|) \equiv 2\sum_{n=0}^{\infty}\frac{1}{(2n+1)\pi}\arctan\left(\frac{|x_1|}{(2n+1)\pi}\right) \times \frac{|x_2|}{|x_2|^2+[(2n+1)\pi]^2}, \tag{B2}$$

The other sum is

$$\sum_n \frac{1}{\omega_n^2}\arctan\left(\frac{y_1}{\omega_n}\right)\arctan\left(\frac{y_2}{\omega_n}\right) = \frac{\text{sign}(y_1y_2)}{T_c^2}s_3\left(\frac{|y_1|}{T_c},\frac{|y_2|}{T_c}\right),$$

where we define

$$s_3(|x_1|,|x_2|) \equiv 2\sum_{n=0}^{\infty}\frac{1}{[(2n+1)\pi]^2}\arctan\left(\frac{|x_1|}{(2n+1)\pi}\right) \times \arctan\left(\frac{|x_2|}{(2n+1)\pi}\right). \tag{B3}$$

In these expressions, both y_1 and y_2 can assume the values $\Omega_0 = \Lambda$, $W_1 = -\mu$, or $W_2 = -\mu + \varepsilon_0$. To proceed with the calculation of Eqs. (B2) and (B3), we use an asymptotic approach similar to that described in Appendix A. In each of the four regions of the two-dimensional parameter space $|x_1| \times |x_2|$ bounded by the lines $|x_1| = 1$ and $|x_2| = 1$ (see Fig. 12), we substitute $\arctan(\frac{|x_i|}{(2n+1)\pi})$ and $\frac{|x_i|}{|x_i|^2+[(2n+1)\pi]^2}$ by their Taylor expansions in powers of $|x_i|$ if $|x_i| \ll 1$, or $1/|x_i|$ if $|x_i| \gg 1$.

When $|x_i| \gg 1$ we decompose the sums over n into two contributions, $\sum_{n=0}^{\infty} f(n) = \sum_{n=0}^{N_i^*} f(n) + \sum_{n=N_i^*+1}^{\infty} f(n)$, where $f(n)$ denotes any function of n. As in Appendix A, $N_i^* = \frac{|x_i|}{2\pi} - \frac{1}{2}$ is defined such that $(2N_i^*+1)\pi = |x_i|$. When both $|x_1| \gg 1$ and $|x_2| \gg 1$, the decomposition is such that $\sum_{n=0}^{\infty} f(n) = \sum_{n=0}^{N_<^*} f(n) + \sum_{n=N_<^*+1}^{N_>^*} f(n) + \sum_{n=N_>^*+1}^{\infty} f(n)$, with $N_<^* = \min\{N_1^*,N_2^*\}$ and $N_>^* = \max\{N_1^*,N_2^*\}$. Therefore, besides the sums already calculated in Eqs. (A3), (A8), and (A9), we also need, for $|x_i| \gg 1$,

$$\sum_{n=N_1^*}^{N_2^*}\frac{1}{[(2n+1)\pi]^k} \sim \begin{cases} \frac{1}{2\pi}\ln\left(\frac{|x_2|}{|x_1|}\right), & \text{if } k=1 \\ \frac{1}{2\pi(k-1)}\left[\frac{1}{|x_1|^{k-1}}-\frac{1}{|x_2|^{k-1}}\right], & \text{if } k\leqslant 0 \text{ or } k>1 \end{cases}. \tag{B4}$$

After a tedious but straightforward calculation, we then find the following asymptotic approximations for Eqs. (B2) and (B3) in each of the four asymptotic regions of the $(|x_1|,|x_2|)$ plane:

$$s_2(|x_1|,|x_2|) \approx \begin{cases} 0, & \text{if} \quad |x_1|, |x_2| \ll 1 \\ \kappa'|x_2|, & \text{if} \quad |x_1| \gg 1, |x_2| \ll 1 \\ \frac{1}{2|x_2|}\ln(\kappa|x_<|) - \frac{|x_1|}{2|x_>|^2} + \frac{|x_2|\,\theta(|x_1|-|x_2|)}{4|x_1|^2}, & \text{if} \quad |x_1|, |x_2| \gg 1 \\ 0, & \text{if} \quad |x_1| \ll 1, |x_2| \gg 1 \end{cases}, \tag{B5}$$

and

$$s_3(|x_1|,|x_2|) \approx \begin{cases} 0, & \text{if} \quad |x_1|,|x_2| \ll 1 \\ \kappa'|x_2|, & \text{if} \quad |x_1| \gg 1, |x_2| \ll 1 \\ \frac{\pi^2}{16} - \frac{(|x_1|+|x_2|)}{2|x_1||x_2|}\ln(\kappa|x_<|) - \frac{1}{2|x_<|} + \frac{|x_<|}{2|x_>|^2}, & \text{if} \quad |x_1|,|x_2| \gg 1 \\ \kappa'|x_1|, & \text{if} \quad |x_1| \ll 1, |x_2| \gg 1 \end{cases}. \tag{B6}$$

Here, we defined the constant $\kappa' = \frac{7\zeta(3)}{8\pi^2} \approx 0.11$ and defined $|x_<| = \min\{|x_1|,|x_2|\}$ and $|x_>| = \max\{|x_1|,|x_2|\}$. Recall that $\zeta(x)$ is the zeta function, $\theta(x)$ is the Heaviside step function and $\kappa \approx 1.13$ is the constant defined in Appendix A.

It is important to note that we treat the approximations we use during the derivation of Eqs. (B5) and (B6) consistently: in all four regions of the parameter space shown in Fig. 12, we kept only terms up to order $\mathcal{O}(|x|^2)$, with $|x| \ll 1$. Note that there is a small sliver region around $|x_1| = |x_2|$ in region 3 where this approximation loses precision as compared to the other regions of the $(|x_1|,|x_2|)$ plane.

The matrix elements of $\delta\hat{A}$, defined in Eq. (53), are given by combinations of Eqs. (B5) and (B6). In each region of the phase diagram shown in Fig. 3, the leading contributions yield for R_1

$$R_1 \sim \begin{cases} \frac{\Omega_0+\mu-\varepsilon_0}{2\Omega_0^2} + \frac{1}{2\Omega_0}\ln\left(\frac{\varepsilon_0-\mu}{\Omega_0}\right), & \text{region I} \\ \frac{4\Omega_0+\mu-2\varepsilon_0}{4\Omega_0^2} + \frac{\mu\,\theta(\varepsilon_0-2\mu)}{4(\varepsilon_0-\mu)^2} - \frac{\varepsilon_0-\mu}{2W_>^2} + \frac{1}{2\Omega_0}\ln\left(\frac{\varepsilon_0-\mu}{\Omega_0}\right) - \frac{1}{2\mu}\ln\left(\frac{\mu}{W_<}\right), & \text{region II} \\ \frac{4\Omega_0-\mu}{4\Omega_0^2} - \frac{1}{2\mu}\ln\left(\frac{\kappa\mu}{T_c}\right) + \frac{1}{2\Omega_0}\ln\left(\frac{\kappa\Omega_0}{T_c}\right), & \text{region III} \\ \frac{4\Omega_0+\mu-2\varepsilon_0}{4\Omega_0^2} + \frac{\mu-\varepsilon_0}{2\mu^2} - \frac{1}{2\mu}\ln\left(\frac{\kappa^2\mu(\mu-\varepsilon_0)}{T_c^2}\right) - \frac{1}{2\Omega_0}\ln\left(\frac{\kappa^2\Omega_0(\mu-\varepsilon_0)}{T_c^2}\right), & \text{region IV} \end{cases}. \tag{B7}$$

For R_2, we find

$$R_2 \sim \begin{cases} \frac{\varepsilon_0-\mu}{4\Omega_0^2} + \frac{1}{2(\varepsilon_0-\mu)}\ln\left(\frac{\kappa(\varepsilon_0-\mu)}{T_c}\right) - \frac{1}{2\Omega_0}\ln\left(\frac{\kappa\Omega_0}{T_c}\right), & \text{region I} \\ \frac{\mu+\varepsilon_0}{4\Omega_0^2} - \frac{\mu}{2W_>^2} + \frac{(\varepsilon_0-\mu)\,\theta(2\mu-\varepsilon_0)}{4\mu^2} + \frac{1}{2(\varepsilon_0-\mu)}\ln\left(\frac{\kappa^2(\varepsilon_0-\mu)W_<}{T_c^2}\right) - \frac{1}{2\Omega_0}\ln\left(\frac{\kappa^2\mu\Omega_0}{T_c^2}\right), & \text{region II} \\ \frac{\Omega_0+\mu}{2\Omega_0^2} + \frac{2\kappa'(\varepsilon_0-\mu)}{T_c^2} - \frac{1}{2\Omega_0}\ln\left(\frac{\kappa^2\mu\Omega_0}{T_c^2}\right), & \text{region III} \\ \frac{\mu+\varepsilon_0}{4\mu^2} + \frac{\mu+\varepsilon_0+4\Omega_0}{4\Omega_0^2} - \frac{1}{2\Omega_0}\ln\left(\frac{\kappa^2\Omega_0\mu}{T_c^2}\right) - \frac{1}{\mu-\varepsilon_0}\ln\left(\frac{\kappa(\mu-\varepsilon_0)}{T_c}\right), & \text{region IV} \end{cases}. \tag{B8}$$

and for S:

$$S \sim \begin{cases} \frac{1}{2(\varepsilon_0-\mu)} - \frac{\varepsilon_0-\mu}{2\Omega_0^2} + \frac{1}{2(\varepsilon_0-\mu)}\ln\left(\frac{\kappa(\varepsilon_0-\mu)}{T_c}\right) - \frac{1}{2\Omega_0}\ln\left(\frac{\kappa\Omega_0^2}{(\varepsilon_0-\mu)T_c}\right), & \text{region I} \\ \frac{2\mu-\varepsilon_0}{2\mu(\varepsilon_0-\mu)} - \frac{\varepsilon_0-2\mu}{2\Omega_0^2} + \frac{1}{2W_<} - \frac{W_<}{2W_>^2} + \frac{\varepsilon_0}{2\mu(\varepsilon_0-\mu)}\ln\left(\frac{\kappa W_<}{T_c}\right) - \frac{1}{2\mu}\ln\left(\frac{\kappa\mu}{T_c}\right) + \frac{1}{2(\varepsilon_0-\mu)}\ln\left(\frac{\kappa(\varepsilon_0-\mu)}{T_c}\right) - \frac{1}{2\Omega_0}\ln\left(\frac{\kappa^2\Omega^2\mu}{(\varepsilon_0-\mu)T_c^2}\right), & \text{region II} \\ \frac{\pi^2}{8T_c} - \frac{2\kappa'(\varepsilon_0-\mu)}{T_c^2} - \frac{1}{2\mu} + \frac{\mu}{2\Omega_0^2} - \frac{1}{2\mu}\ln\left(\frac{\kappa\mu}{T_c}\right) - \frac{1}{2\Omega_0}\ln\left(\frac{\kappa^3\Omega_0^2\mu}{T_c^3}\right), & \text{region III} \\ \frac{\pi^2}{4T_c} - \frac{1}{\mu-\varepsilon_0} - \frac{\varepsilon_0}{2\mu^2} + \frac{2\mu-\varepsilon_0}{2\Omega_0^2} - \frac{1}{2\Omega_0}\ln\left(\frac{\kappa^4\Omega_0^2\mu(\mu-\varepsilon_0)}{T_c^4}\right) - \frac{1}{2\mu}\ln\left(\frac{\kappa^2\mu(\mu-\varepsilon_0)}{T_c^2}\right) - \frac{1}{\mu-\varepsilon_0}\ln\left(\frac{\kappa(\mu-\varepsilon_0)}{T_c}\right), & \text{region IV} \end{cases}. \tag{B9}$$

where, $W_< \equiv \min\{|W_1|,|W_2|\}$ and $W_> \equiv \max\{|W_1|,|W_2|\}$. The order of the terms in the expressions for R_1, R_2 and S are also consistent with those in Eqs. (B5) and (B6).

APPENDIX C: $T_c(\mu)$ AND $\partial T_c/\partial \tau_{ij}^{-1}$ IN THE DILUTE REGIME

Here, we provide more details about the calculation of the analytic asymptotic expression of T_c, as well as its suppression rate by interband nonmagnetic impurity scattering, $\frac{\partial T_c}{\partial \tau_{\rm inter}^{-1}}|_{\tau_{\rm inter}^{-1}=0}$, as function of the chemical potential.

Recalling that we denote by $\alpha(T)$ the largest eigenvalue of $\hat{\lambda}\hat{A}_d$, where $\hat{A}_d$ is defined in Eq. (51), it follows that, similar to Sec. II B, finding $T_c(\mu)$ involves solving a transcendental algebraic equation $\alpha = 1$, with

$$\alpha = \tfrac{1}{2}[a_{11} + a_{22} + \sqrt{(a_{11} - a_{22})^2 + 4a_{12}a_{21}}], \tag{C1}$$

where we defined, in terms of the analytic expressions for R_i and S calculated in Appendix B:

$$\begin{aligned} a_{11} &= \lambda_{11}\left[A_1 + \frac{\tau_{\rm inter}^{-1}}{2\pi}(R_1 - S)\right] + \frac{\tau_{\rm inter}^{-1}}{2\pi}\lambda_{12}S, \quad a_{12} = \lambda_{12}\left[A_2 + \frac{\tau_{\rm inter}^{-1}}{2\pi}(R_2 - S)\right] + \frac{\tau_{\rm inter}^{-1}}{2\pi}\lambda_{11}S, \\ a_{21} &= \lambda_{12}\left[A_1 + \frac{\tau_{\rm inter}^{-1}}{2\pi}(R_1 - S)\right] + \frac{\tau_{\rm inter}^{-1}}{2\pi}\lambda_{22}S, \quad a_{22} = \lambda_{22}\left[A_2 + \frac{\tau_{\rm inter}^{-1}}{2\pi}(R_2 - S)\right] + \frac{\tau_{\rm inter}^{-1}}{2\pi}\lambda_{12}S, \end{aligned} \tag{C2}$$

with $A_1 = (\hat{A}_c)_{11}$ and $A_2 = (\hat{A}_c)_{22}$. The resulting $T_c(\mu)$, for both attractive ($\lambda_{12} > 0$) and repulsive ($\lambda_{12} < 0$) interband superconducting interaction and its comparison with the numeric solution of the gap equations are shown in Fig. 8.

Once we know $T_c(\mu)$, it is straightforward to compute $\frac{\partial T_c}{\partial \tau_{\rm inter}^{-1}}$ from Eq. (31). It follows that the different terms entering Eq. (31), also in terms of the analytical expressions for R_i and S, are given by

$$\left\langle \alpha_L^{(0)} \middle| \frac{\partial(\hat{\lambda}\hat{A}_d)}{\partial \tau_{\rm inter}^{-1}} \middle| \alpha_R^{(0)} \right\rangle = \frac{1}{2\pi}\left\{(1 - \lambda_{11}A_2)\left[(R_1 - S)\left(\lambda_{11} - \lambda_{11}^2A_2 + \lambda_{12}^2A_2\right) + \lambda_{12}S(1 + \lambda_{11}A_1)\right] + \lambda_{12}^2A_1(R_2 - S + \lambda_{12}SA_2)\right\}, \tag{C3}$$

and

$$\left.\frac{\partial \alpha_0}{\partial T}\right|_{T=T_c} = \frac{1}{2 - \lambda_{11}(A_1 + A_2)} \sum_{j=1}^{2} \left(\lambda_{11} - \lambda_{11}^2A_j + \lambda_{12}^2A_j\right) \left.\frac{\partial A_{\bar{j}}}{\partial T}\right|_{T=T_c}, \tag{C4}$$

as well as

$$\left\langle \alpha_L^{(0)} \middle| \alpha_R^{(0)} \right\rangle = (1 - \lambda_{11}A_2)^2 + \lambda_{12}^2A_1A_2. \tag{C5}$$

In the previous equations, $A_i \equiv (\hat{A}_c)_{ii}$ and we set $\lambda_{11} = \lambda_{22}$ for simplicity. The resulting $\frac{\partial T_c}{\partial \tau_{\rm inter}^{-1}}|_{\tau_{\rm inter}^{-1}=0}$, for both attractive and repulsive interband superconducting interactions, are shown in Fig. 9.

[1] H. Suhl, T. B. Matthias, and R. L. Walker, Phys. Rev. Lett. **3**, 552 (1959).
[2] V. A. Moskalenko, Fiz. Met. Mettaloved. **8**, 503 (1959).
[3] A. Y. Liu, I. I. Mazin, and J. Kortus, Phys. Rev. Lett. **87**, 087005 (2001).
[4] M. Marz, G. Goll, W. Goldacker, and R. Lortz, Phys. Rev. B **82**, 024507 (2010).
[5] T. Yokoya, T. Kiss, A. Chainani, S. Shin, M. Nohara, and H. Takagi, Science **294**, 2518 (2001).
[6] H. Ding, P. Richard, K. Nakayama, K. Sugawara, T. Arakane, Y. Sekiba, A. Takayama, S. Souma, T. Sato, T. Takahashi, Z. Wang, X. Dai, Z. Fang, G. F. Chen, J. L. Luo, and N. L. Wang, Europhys. Lett. **83**, 47001 (2008).
[7] A. P. Mackenzie, S. R. Julian, A. J. Diver, G. J. McMullan, M. P. Ray, G. G. Lonzarich, Y. Maeno, S. Nishizaki, and T. Fujita, Phys. Rev. Lett. **76**, 3786 (1996).
[8] P. M. C. Rourke, M. A. Tanatar, C. S. Turel, J. Berdeklis, C. Petrovic, and J. Y. T. Wei, Phys. Rev. Lett. **94**, 107005 (2005).
[9] X. Lin, G. Bridoux, A. Gourgout, G. Seyfarth, S. Krämer, M. Nardone, B. Fauqué, and K. Behnia, Phys. Rev. Lett. **112**, 207002 (2014).
[10] G. Binnig, A. Baratoff, H. E. Hoenig, and J. G. Bednorz, Phys. Rev. Lett. **45**, 1352 (1980).
[11] A. Joshua, S. Pecker, J. Ruhman, E. Altman, and S. Ilani, Nat. Commun. **3**, 1129 (2012).
[12] S. E. Rowley, L. J. Spalek, R. P. Smith, M. P. M. Dean, M. Itoh, J. F. Scott, G. G. Lonzarich, and S. S. Saxena, Nat. Phys. **10**, 367 (2014).
[13] J. M. Edge, Y. Kedem, U. Aschauer, N. A. Spaldin, and A. V. Balatsky, Phys. Rev. Lett. **115**, 247002 (2015).
[14] L. P. Gor'kov, arXiv:1610.02062.
[15] J. Ruhman and P. A. Lee, Phys. Rev. B **94**, 224515 (2016).
[16] J. R. Arce-Gamboa and G. G. Guzmán-Verri, arXiv:1801.08736.
[17] M. S. Scheurer and J. Schmalian, Nat. Commun. **6**, 6005 (2015).
[18] D. V. Efremov, M. M. Korshunov, O. V. Dolgov, A. A. Golubov, and P. J. Hirschfeld, Phys. Rev. B **84**, 180512(R) (2011).

[19] S. Maiti and A. V. Chubukov, Phys. Rev. B **87**, 144511 (2013).
[20] E. Babaev and M. Speight, Phys. Rev. B **72**, 180502(R) (2005).
[21] J. Geyer, R. M. Fernandes, V. G. Kogan, and J. Schmalian, Phys. Rev. B **82**, 104521 (2010).
[22] L. Komendova, Y. Chen, A. A. Shanenko, M. V. Milosevic, and F. M. Peeters, Phys. Rev. Lett. **108**, 207002 (2012).
[23] L. Komendova, A. V. Balatsky, and A. M. Black-Schaffer, Phys. Rev. B **92**, 094517 (2015).
[24] M. Silaev and E. Babaev, Phys. Rev. B **84**, 094515 (2011).
[25] I. M. Lifshitz, Sov. Phys. JETP **11**, 1130 (1960).
[26] A. Bianconi, Sol. State Commun. **89**, 933 (1994).
[27] R. M. Fernandes, J. T. Haraldsen, P. Wölfle, and A. V. Balatsky, Phys. Rev. B **87**, 014510 (2013).
[28] A. Bianconi, D. Innocenti, A. Valletta, and A. Perali, J. Phys.: Conf. Ser. **529**, 012007 (2014).
[29] A. V. Chubukov, I. Eremin, and D. V. Efremov, Phys. Rev. B **93**, 174516 (2016).
[30] J. M. Edge and A. V. Balatsky, J. Supercond. Nov. Magn. **28**, 2373 (2015).
[31] X. Chen, V. Mishra, S. Maiti, and P. J. Hirschfeld, Phys. Rev. B **94**, 054524 (2016).
[32] Y. Bang, New J. Phys. **16**, 023029 (2014).
[33] X. Chen, S. Maiti, A. Linscheid, and P. J. Hirschfeld, Phys. Rev. B **92**, 224514 (2015).
[34] D. Innocenti, N. Poccia, A. Ricci, A. Valletta, S. Caprara, A. Perali, and A. Bianconi, Phys. Rev. B **82**, 184528 (2010).
[35] K. W. Song and A. E. Koshelev, Phys. Rev. B **95**, 174503 (2017).
[36] D. Valentinis, D. van der Marel, and C. Berthod, Phys. Rev. B **94**, 024511 (2016).
[37] C. Liu, A. D. Palczewski, R. S. Dhaka, T. Kondo, R. M. Fernandes, E. D. Mun, H. Hodovanets, A. N. Thaler, J. Schmalian, S. L. Bud'ko, P. C. Canfield, and A. Kaminski, Phys. Rev. B **84**, 020509(R) (2011).
[38] Y. Nakajima, R. Wang, T. Metz, X. Wang, L. Wang, H. Cynn, S. T. Weir, J. R. Jeffries, and J. Paglione, Phys. Rev. B **91**, 060508(R) (2015).
[39] T. V. Trevisan, M. Schütt, and R. M. Fernandes, Phys. Rev. Lett. **121**, 127002 (2018).
[40] D. J. Bergmann and D. Rainer, Z. Phys. **263**, 59 (1973).
[41] J. Kang and R. M. Fernandes, Phys. Rev. B **93**, 224514 (2016).
[42] A. A. Golubov and I. I. Mazin, Phys. Rev. B **55**, 15146 (1997).
[43] Y. Wang, A. Kreisel, P. J. Hirschfeld, and V. Mishra, Phys. Rev. B **87**, 094504 (2013).
[44] M. S. Scheurer, M. Hoyer, and J. Schmalian, Phys. Rev. B **92**, 014518 (2015).